Physics – Uspekhi **64** (2) 157 – 174 (2021)

REVIEWS OF TOPICAL PROBLEMS PACS numbers: 61.20.Lc, 61.20.Ne, **66.20. – d**, 66.30.jj

Collective contributions to self-diffusion in liquids

N P Malomuzh, K S Shakun

DOI: https://doi.org/10.3367/UFNe.2020.05.038759

Contents

Abstract. The present work is devoted to describing the current state of the collective transport theory in liquids. In this connection, the results of MD-modeling of the root mean square displacement and the velocity autocorrelation function of a molecule (VACFM) at large enough times are discussed. The characteristic function allowing one to estimate the relative value of collective contributions to the self-diffusion coefficient is introduced and studied in detail. Low-frequency spectra of the VACFM are used to determine the Maxwell relaxation time, playing the key role in the approach presented. The possibility of determining the binodal and spinodal positions by the temperature dependences of self-diffusion coefficients on isochores is considered.

Keywords: self-diffusion, collective effects, velocity autocorrelation function, metastable states, spinodal

N P Malomuzh [(1)], **K S Shakun** [(2)]
I I Mechnikov Odessa National University,
Department of Theoretical Physics and Astronomy,
ul. Dvoryanskaya 2, 65026 Odessa, Ukraine
E-mail: [(1)] mnp@onu.edu.ua, [(2)] shks.solomon@gmail.com

Received 26 December 2019, revised 26 April 2020
Uspekhi Fizicheskikh Nauk **191** (2) 163 – 181 (2021)
Translated by S D Danilov

1. Introduction

The main concepts of and the first results in the theory of collective transport of molecules in liquids were outlined in a series of papers [1–4] initiated by I Z Fisher. February 2019 marked the 100th anniversary of his birth, and this year, 2021, will mark the 50th anniversary of the publication of his seminal paper [1] on the problem of collective contribution to the self-diffusion coefficient. In this regard, we would like to present the most important results obtained by exploring this question over past years.

An important impetus to the development of collective transport theory were studies by Alder and Wainwright [5–8] where, using methods of molecular dynamics, it was found that the velocity autocorrelation function (VACF) of a molecule (VACFM) of liquid $\phi_{\mathbf{V}}(t) = \langle \mathbf{V}(t)\mathbf{V}(0)\rangle$ at large enough time intervals ($t \gg a/V_T \sim (0.5-1)\times 10^{-12}$ s, where

a is the mean distance between nearest neighbors and V_T is the mean thermal motion velocity of molecules) has a universal power-law asymptotic behavior,

$$\phi_{\mathbf{V}}(t) \to \frac{A}{t^{3/2}} . \tag{1}$$

In the following years, this result was confirmed in numerous computer experiments [9–13]. The universal character of the decay of VACFM soon became the subject of systematic research in Refs [14–22], which showed that it is the result of a diffusive decay of vortical hydrodynamic modes in liquids. In this case, the coefficient A also has a universal form,

$$A = \frac{k_{\mathrm{B}}T}{4\rho(\pi\nu)^{3/2}} , \tag{2}$$

where T, ρ, and ν are, respectively, the temperature, mass density, and shear viscosity of the liquid, and k_{B} is the Boltzmann constant. It is important to stress that the best problem treatment is offered in Fisher's work [1], where it was assumed that the slowest components of the thermal motion velocity of molecules are governed by the velocity $\mathbf{V}_{\mathrm{L}}(t)$ of a liquid (Lagrangian) particle containing this molecule in the field of thermal hydrodynamic fluctuations, i.e.,

$$\mathbf{V}(t) = \mathbf{V}_{\mathrm{L}}(t) + \mathbf{V}_{\mathrm{r}}(t) . \tag{3}$$

The component $\mathbf{V}_{\mathrm{r}}(t)$ is assumed to be due to faster modes of thermal motion of nonhydrodynamic origin. As a consequence, the asymptotic behavior of $\phi_{\mathbf{V}}(t)$ is defined by the VACF of Lagrangian particle $\phi_{\mathbf{V}_{\mathrm{L}}}(t) = \langle \mathbf{V}_{\mathrm{L}}(t)\mathbf{V}_{\mathrm{L}}(0)\rangle$,

$$\phi_{\mathbf{V}}(t) \to \phi_{\mathbf{V}_{\mathrm{L}}}(t) , \quad t \gg \frac{a}{V_T} . \tag{4}$$

This triggered interest in developing the Lagrangian theory of hydrodynamic fluctuations. In the first outline of this theory in Ref. [1], it was assumed that

$$\mathbf{V}_{\mathrm{L}}(t) = \mathbf{u}(\mathbf{r}, t)|_{\mathbf{r}=\mathbf{r}_{\mathrm{L}}(t)} , \tag{5}$$

where $\mathbf{u}(\mathbf{r}, t)$ is the ordinary (Eulerian) hydrodynamic velocity in liquids and $\mathbf{r}_{\mathrm{L}}(t)$ is the position vector of the Lagrangian particle center. The correlation functions (CFs) $\psi_{\mathbf{u}}(\mathbf{r}, t) = \langle \mathbf{u}(\mathbf{r}, t)\mathbf{u}(0, 0)\rangle$ of Eulerian velocity field $\mathbf{u}(\mathbf{r}, t)$ were already well studied by that time [23–26], such that Ref. [1] aimed at finding a link between the VACF of a Lagrangian particle $\phi_{\mathbf{V}_{\mathrm{L}}}(t)$ and the Eulerian CF $\psi_{\mathbf{u}}(\mathbf{r}, t)$. The respective operator $\hat{F}$ linking them, which was established in Refs [1, 2],

$$\phi_{\mathbf{V}_{\mathrm{L}}}(t) = \hat{F}\psi_{\mathbf{u}}(\mathbf{0}, t) , \tag{6}$$

was a sum of contributions obtained by differencing over the raising powers of $\partial/\partial t$.

A weakness of the proposed approach was the fact that the CF $\psi_{\mathbf{u}}(\mathbf{0}, t) \to \infty$ for $t \to 0$, and application of a differencing operator to it only exacerbated this. In addition, it is clear that for $t \to 0$ the Lagrangian particle VACF $\phi_{\mathbf{V}_{\mathrm{L}}}(t)$ should tend to the quantity

$$\phi_{\mathbf{V}_{\mathrm{L}}}(0) = \frac{3k_{\mathrm{B}}T}{m_{\mathrm{L}}} , \quad m_{\mathrm{L}} = \frac{4\pi}{3} r_{\mathrm{L}}^3 \rho , \tag{7}$$

where m_{L} is the particle mass.

This and some other problems were overcome in an approach proposed in Refs [27–30] where the key role is played by the redefinition of link (5) between the Lagrangian particle velocity and the Eulerian velocity field,

$$\mathbf{V}_{\mathrm{L}}(t) = \frac{1}{v_{\mathrm{L}}} \int_{v_{\mathrm{L}}} \mathbf{u}\big(\mathbf{r}_{\mathrm{L}}(t) + \mathbf{r}', t\big)\, \mathrm{d}\mathbf{r}' , \tag{8}$$

where $v_{\mathrm{L}} = (4\pi/3)\, r_{\mathrm{L}}^3$ is the Lagrangian particle volume. These studies also constructed an integral operator $\hat{L}$ allowing one to move from CF $\psi_{\mathbf{u}}(\mathbf{r}, t)$ to VACF $\phi_{\mathbf{V}_{\mathrm{L}}}(t)$ of the Lagrangian particle,

$$\phi_{\mathbf{V}_{\mathrm{L}}}(t) = \hat{L}\psi_{\mathbf{u}}(\mathbf{r}, t) . \tag{9}$$

In this approach, VACF $\phi_{\mathbf{V}_{\mathrm{L}}}(t)$ of the Lagrangian particle proves to be rigorously defined on the entire time axis ($0 \leqslant t < \infty$), automatically satisfies condition (7), and naturally passes to the long-time asymptotic form that follows from the approach of Fisher [1, 2] and other authors [13, 16, 20, 31–38]. Note that at the same time the Lagrangian theory of thermal hydrodynamic fluctuations was perfected, a theory dealing with the correlation functions of Eulerian variables in hydrodynamics was also advanced further [35, 36].

Importantly, in his paper [1], I Z Fisher does not limit himself exclusively to an analysis of the long-time asymptotic form of the VACFM, but introduces the important notion of a collective component D_{c} in the self-diffusion coefficient and derives a concrete expression for this component. The necessity of this notion had already been mentioned earlier in Ref. [39] exploring thermal neutron scattering.

The origin of the collective component in the self-diffusion coefficient is naturally illustrated by trajectories of passengers at underground transfer stations in the morning rush hour. Each passenger aims to change to the station needed, but, being surrounded by a dense crowd, only squeezes between the nearest neighbors and drifts together with them to the side that corresponds to the strongest passenger flow. The transport of a passive passenger by local flows occurring at transfer stations is a precise illustration of collective transport in liquids.

In liquids, each molecule not only moves relative its nearest neighbors but also drifts together with them in the field of fluctuating hydrodynamic flows. In this respect, it should be stressed that, while the VACFM falls in the class of single-particle characteristics of the system, the character of its temporal dependence is determined by the details of the dynamics of the entire particle set. This remark also remains valid for the mean square particle displacement.

The collective component in the self-diffusion coefficient of molecules can be naturally estimated based on the self-diffusion coefficient D_{L} for a Lagrangian particle of a certain size. References [27–29] show that $D_{\mathrm{L}} = 1/3 \int_0^\infty \phi_{\mathbf{V}_{\mathrm{L}}}(t)\, \mathrm{d}t$ of a Lagrangian particle with radius r_{L} is expressed as

$$D_{\mathrm{L}} = \frac{k_{\mathrm{B}}T}{5\pi\eta r_{\mathrm{L}}} , \tag{10}$$

where $\eta = \nu\rho$ is the dynamical viscosity.

The collective component in the self-diffusion coefficient of molecules D_{c} is naturally defined by the relationship

$$D_{\mathrm{c}} = D_{\mathrm{L}}|_{r_{\mathrm{L}}=r_*} , \tag{11}$$

where r_* is an appropriate radius of the Lagrangian particle. The radius is defined as the minimum value of hydrodynamic

correlation radius $r_H = 2\sqrt{\nu t}$ for vortical components of the fluctuating velocity field. Obviously, the minimum value of r_H is realized for $t = \tau_M$, where τ_M is the Maxwell relaxation time (MRT) of viscous stresses, i.e.,

$$r_* = 2\sqrt{\nu\tau_M}\,. \tag{12}$$

At shorter time intervals, system behavior is governed by elastic modes that are oscillating and do not contribute to the self-diffusion coefficient of molecules. As a result, the collective component of this coefficient takes the form [40]

$$D_c = \frac{k_B T}{10\pi\eta\sqrt{\nu\tau_M}}\,. \tag{13}$$

In Fisher's paper [1], a somewhat smaller value of the numerical factor was obtained,

$$D_c^{(F)} = \frac{k_B T}{16\pi\eta\sqrt{\nu\tau_M}}\,, \tag{14}$$

which is explained by the difference between $\phi_{\mathbf{V}_L}(t)$ and $\psi_{\mathbf{u}}(\mathbf{0}, t)$ taken in [1] for $\phi_{\mathbf{V}_L}(t)$, as $t \to 0$. More precisely, the δ-like contribution entering $\psi_{\mathbf{u}}(\mathbf{0}, t)$ (see Refs [1, 41]) was omitted, even though it leads to a nonzero contribution to the self-diffusion coefficient of a molecule.

From the discussion above, it follows that the self-diffusion coefficient of molecules in liquids is the sum of the collective component D_c and the contribution D_r due to random displacement of molecules on molecular scales,

$$D_s = D_c + D_r\,. \tag{15}$$

The first estimates of the temperature dependence of D_c, as well as the relative magnitude D_c/D_s of the collective contribution, where D_s is given by experimental estimates of the self-diffusion coefficient, were proposed in Refs [40–49]. These estimates were obtained under the assumption that the MRT is described by the Maxwell model

$$\tau_M = \frac{\eta}{G} \tag{16}$$

and that the high-frequency elasticity modulus G in liquids is determined with the help of computer modeling. In the case of argon, the magnitude of G was estimated in Refs [50–52] in the 1970s–1980s only for several temperature values close to the argon triple point. That is why to obtain MRT at other temperatures in the liquid argon existence interval it was supposed that 1) τ_M stays independent of temperature and 2) the high-frequency shear modulus is also independent of temperature. In the first case, the lower bounds on D_c/D_s were obtained, and in the second case, the upper ones. In the case of water and liquid metals, it was assumed that the magnitude of G stays close to the shear modulus in the same system if it is in the crystal or amorphous state [50].

Based on such assumptions, it has been shown that in argon the ratio D_c/D_s increases from $D_c/D_s \approx 0.1$ in the vicinity of the triple point to 0.2–0.3 [46, 47, 49] in the vicinity of the critical point. Similar behavior was observed for liquid metals. For water, the ratio D_c/D_s was noticeably smaller in the vicinity of its triple point, $D_c/D_s \approx 0.03 - 0.05$, and tended to 0.2 for increasing temperatures.

Unfortunately, the degree of reliability of these estimates left much to be desired, since it depended entirely on how accurately the MRT was determined.

An important step in the clarification of the role of collective contributions in self-diffusion was made in studies by L A Bulavin [53–55] at the end of the 1980s. By processing experimental results on thermal neutron scattering in electrolytes by formulas from Ref. [46] with additional account for collective transport, it was shown that the magnitude of the ratio D_c/D_s is on the order of 0.2–0.3 for water molecules. This explicitly pointed to the importance of collective transport, at least in solutions of electrolytes.

These facts markedly raised the significance of the MRT as concerns the role of collective molecule drift in liquids, which we discuss here. This is why we would like to present below our main results on this problem, which were obtained over the last few years [56]. In addition, we will point to a general method allowing the ratio D_c/D_s to be estimated with the help of molecular dynamics, without resorting to concrete computations of the MRT. One more motive impelling us to write this review is an underestimation of the role of collective contributions to the self-diffusion coefficient in the western literature [57–60]. We also pay special attention to the possibility of determining the position of the spinodal separating the liquid and gaseous system states. Our results will be illustrated first and foremost by examples of argon and water. It will be shown that the thermal motion of molecules in low-molecular liquids has nothing in common with the activation mechanism.

2. Qualitative features of the hydrodynamic mechanism of collective transport in liquids

In this section, we discuss basic qualitative details of the collective drift of molecules in liquids.

2.1 Universality of the collective drift of molecules

The most important distinction between liquids and solids, to which they are close if judged by density, is their fluidity, owing to which there are fluctuating hydrodynamic fields in liquids, whose spatio-temporal evolution is irreversible. A random collective drift of liquid (Lagrangian) particles in such fields is in many respects analogous to the random walks of a Brownian particle (the distinction lies only in the details of the boundary conditions).

In other words, collective contributions in the self-diffusion coefficient of molecules are as natural and universal as the mechanism of self-diffusion for Brownian particles.

2.2 Role of longitudinal and transverse modes of the hydrodynamic velocity field in the formation of collective self-diffusion

In the general case, the velocity field in a liquid medium is the sum of two components [1, 14],

$$\mathbf{u}(\mathbf{r}, t) = \mathbf{u}_s(\mathbf{r}, t) + \mathbf{u}_p(\mathbf{r}, t)\,, \tag{17}$$

where the first one describes vortical type motions and the second one is a potential type,

$$\operatorname{div}\mathbf{u}_s(\mathbf{r}, t) = 0\,, \quad \operatorname{rot}\mathbf{u}_p(\mathbf{r}, t) = 0\,. \tag{18}$$

The potential component in velocity fields is directly related to variations in density and temperature. These variations generally imply forward and return motions in the medium (sound waves), which can only lead to negligibly

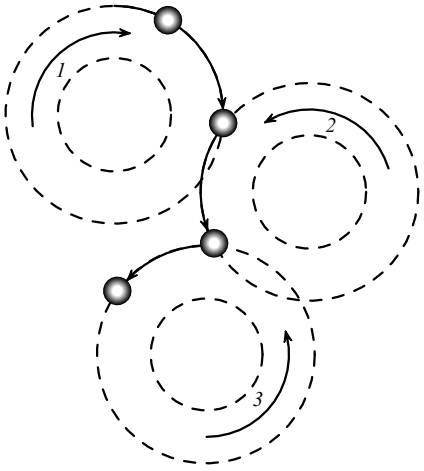

Figure 1. Diagrams of the mechanism of collective transport by fluctuating vortices.

small displacements in the medium and, as a consequence, to similarly small contributions to the collective component of the self-diffusion coefficient. In contrast, vortical displacements lead to a systematic drift of molecules in liquids (Fig. 1).

Originally, a molecule in a medium (circle in Fig. 1) is trapped in vortex *1* and carried over some distance. Vortex *1* then decays, but vortex *2* happens to occur in the vicinity of this molecule, carrying it further over some distance. Its subsequent displacements proceed in a similar manner.

An important circumstance is that the solenoidal (transverse) component of the fluctuating velocity field is described by the diffusion equation

$$\frac{\partial \mathbf{u}_\mathrm{s}(\mathbf{r},t)}{\partial t} = \nu \Delta \mathbf{u}_\mathrm{s}(\mathbf{r},t) \tag{19}$$

or its generalization

$$\frac{\partial \mathbf{u}_\mathrm{s}(\mathbf{r},t)}{\partial t} + \tau_\mathrm{M} \frac{\partial^2 \mathbf{u}_\mathrm{s}(\mathbf{r},t)}{\partial t^2} = \nu \Delta \mathbf{u}_\mathrm{s}(\mathbf{r},t)\,, \tag{20}$$

transforming into diffusion equation (19) at sufficiently large times ($t \gg \tau_\mathrm{M}$) and into a wave equation in short times ($t \ll \tau_\mathrm{M}$), where Δ is the Laplace operator. Fluctuating vortical perturbations are described by the same equations.

Note that equation (20) corresponds to the well-known Maxwell model of the frequency dispersion of kinematic shear viscosity in liquids:

$$\nu(\omega) = \frac{\nu(0)}{1 + \mathrm{i}\omega\tau_\mathrm{M}}\,.$$

We stress that, in what follows, we will only use the definition of MRT given by the last relationship and equations (16) and (20). The definition of MRT by Green–Kubo formulas [61–63] does not fully agree with (16) and (20) (see Refs [64–69]).

2.3 Features of the collective drift of molecules

The mean square displacement (MSD) of a molecule over time t is defined by the equation

$$\Gamma(t) = \left\langle \left(\int_0^t \mathbf{V}(t')\,\mathrm{d}t' \right)^2 \right\rangle \Rightarrow 2\int_0^t (t-t')\phi_\mathbf{V}(t')\,\mathrm{d}t'\,. \tag{21}$$

Using expression (3) for the velocity of a molecule, $\Gamma(t)$ can be written as

$$\Gamma(t) = \Gamma_\mathrm{c}(t) + \Gamma_\mathrm{r}(t)\,, \tag{22}$$

where

$$\Gamma_\mathrm{c}(t) = 2t\int_0^t \phi_{\mathbf{V}_\mathrm{c}}(t')\,\mathrm{d}t' - 2\int_0^t t'\phi_{\mathbf{V}_\mathrm{c}}(t')\,\mathrm{d}t'\,, \tag{23}$$

$$\Gamma_\mathrm{r}(t) = 2t\int_0^t \phi_{\mathbf{V}_\mathrm{r}}(t')\,\mathrm{d}t' - C_\mathrm{r}\,, \quad C_\mathrm{r} = 2\int_0^t t'\phi_{\mathbf{V}_\mathrm{r}}(t')\,\mathrm{d}t\,. \tag{24}$$

Here, $\phi_{\mathbf{V}_\mathrm{c}}(t)$ is the VACF of a Lagrangian particle with an appropriate radius r_*, and $\phi_{\mathbf{V}_\mathrm{r}}(t)$ is the contribution to the VACF of the same particle due to small-scale modes of thermal motion of the molecule. It is taken into account that the components $\mathbf{V}_\mathrm{c}$ and $\mathbf{V}_\mathrm{r}$ are statistically independent, $\langle \mathbf{V}_\mathrm{c}(t)\mathbf{V}_\mathrm{r}(0)\rangle = 0$. Since, for $t \gg a/V_T$,

$$\int_0^t \phi_{\mathbf{V}_\mathrm{c}}(t')\,\mathrm{d}t' \to 3D_\mathrm{c}\,, \quad \int_0^t \phi_{\mathbf{V}_\mathrm{r}}(t')\,\mathrm{d}t' \to 3D_\mathrm{r}\,,$$

and also $\phi_{\mathbf{V}_\mathrm{c}}(t) \to A/t^{3/2}$, from (22)–(24) it follows that

$$\Gamma(t) = C + 6D_\mathrm{s}t\left[1 - \frac{10}{3\pi^{1/2}}\frac{D_\mathrm{c}}{D_\mathrm{s}}\left(\frac{\tau_\mathrm{M}}{t}\right)^{1/2} + \ldots\right], \tag{25}$$

where $C \approx C_\mathrm{r}$ ($t = \infty$). It should be stressed that vortical hydrodynamic modes creating the power-law long-time asymptotic form (1) of a VACFM turn out to also be responsible for the appearance of the square-root contribution in its MSD. The relative value of this contribution is proportional to the collective component D_c of the self-diffusion coefficient. The existence of the square-root contribution in the MSD is also mentioned in Ref. [70]; however, it is introduced there only to describe more accurately the results of molecular-dynamical (MD) modeling of the MSD of a molecule.

In dimensionless variables $x = t/\tau_\mathrm{M}$, $\tilde{\Gamma}(x) = \Gamma(t)/(6D_\mathrm{s}\tau_\mathrm{M})$, and $\tilde{C} = C/(6D_\mathrm{s}\tau_\mathrm{M})$, formula (25) for $x^{1/2} \gg 1$ can be rewritten in the form

$$\frac{D_\mathrm{c}}{D_\mathrm{s}} = F\,, \quad F = \lim_{x\to\infty} F(x)\,,$$
$$F(x) = \frac{3\pi^{1/2}}{10}x^{1/2}\left(1 - \frac{\tilde{\Gamma}(x)}{x}\right), \tag{26}$$

where it is taken into account that for such x the dimensionless mean square displacement of a molecule proves to be much larger than the constant $\tilde{C}$ ($\tilde{\Gamma}(x) \gg \tilde{C}$).

The function $F(x)$ has the sense of a characteristic function describing the manifestation of the collective drift of molecules in the MSD. Owing to the isolation of the square root contribution, a fundamental possibility appears of determining the ratio $D_\mathrm{c}/D_\mathrm{s}$ by values of $F_\mathrm{MD}(x)$ computed in numerical experiments. Since the values of $F_\mathrm{MD}(x)$ obtained in different series of computer computations slightly differ from each other, for our goal, we need to apply averaging over different realizations,

$$\frac{D_\mathrm{c}}{D_\mathrm{s}} = \mathrm{Aver}\,F_\mathrm{MD}(x)\,, \quad x^{1/2} \gg 1\,, \tag{27}$$

where

$$F_\mathrm{MD}(x) = \frac{3\pi^{1/2}}{10}x^{1/2}\left(1 - \frac{\tilde{\Gamma}_\mathrm{MD}(x)}{x}\right),$$

$\tilde{\Gamma}_{\rm MD}(x)$ is the MSD of a molecule obtained in computer experiments, and Aver indicates the related averaging operation. We should mention that with an increase in x increasingly more computational errors are accumulated, so that the values of x should be bounded from above by dimensionless times $x_{\rm u}$ of dynamic system memory. In ordinary units, $t_{\rm u}({\rm Ar}) \approx 20$ ps and $t_{\rm u}({\rm H_2O}) \approx 12$ ps (see Section 5.2 and Appendix 1).

When this method is applied to determine the ratio $D_{\rm c}/D_{\rm s}$, a very important circumstance is that its magnitude does not depend on the precise value of MRT $\tau_{\rm M}$. In fact, any value of $\tau_{\rm M}$ can be used if it guarantees that $x^{1/2} \gg 1$.

Since the self-diffusion coefficient in liquids can be estimated with an acceptable accuracy by the Einstein formula $D_{\rm s} = k_{\rm B}T/(6\pi\eta r_{\rm p})$, the fraction of the collective component of the self-diffusion coefficient is defined, on the order of magnitude, by the ratio of the effective radius of molecule $r_{\rm p}$ to the appropriate Lagrangian particle radius,

$$D_{\rm c} \approx \frac{3}{5}\frac{r_{\rm p}}{\sqrt{v\tau_{\rm M}}} D_{\rm s}\,. \tag{28}$$

The numerical value of the ratio $r_{\rm p}/\sqrt{v\tau_{\rm M}} \equiv 2r_{\rm p}/r_*$, where r_* is the appropriate radius of the Lagrangian particle (see (12)), substantially depends on temperature and, within the assumptions mentioned above on the magnitude and temperature dependence of the MRT, varies within 0.05–0.25. This is equivalent to the statement that the Lagrangian particle comprises 64 molecules.

3. General structure of velocity autocorrelation function of a molecule in liquids and its spectrum

In agreement with the discussion in the Introduction and Section 2, VACFM $\phi_{\mathbf{V}}(t) = \langle \mathbf{V}(t)\mathbf{V}(0)\rangle$ has the following structure:

$$\phi_{\mathbf{V}}(t) = \phi_{\mathbf{V}}^{\rm M}(t) + \phi_{\mathbf{V}}^{\rm H}(t)\,, \tag{29}$$

where $\phi_{\mathbf{V}}^{\rm M}(t)$ is the component coming from short-lived molecular modes, and $\phi_{\mathbf{V}}^{\rm H}(t)$ is the component with a hydrodynamic nature.

The properties of $\phi_{\mathbf{V}}^{\rm H}(t)$ are studied in detail in [1, 14], where it is shown that

$$\phi_{\mathbf{V}}^{\rm H}(t) = \phi_{\mathbf{V}}^{\rm S}(t) + \phi_{\mathbf{V}}^{\rm P}(t)\,, \tag{30}$$

where the first and second terms correspond to the vortical and potential modes. The behavior of vortical contribution $\phi_{\mathbf{V}}^{\rm S}(t)$ is governed by hydrodynamic equation (20), which leads to further specification in the structure of $\phi_{\mathbf{V}}^{\rm S}(t)$,

$$\phi_{\mathbf{V}}^{\rm S}(t) = \phi_{\mathbf{V}}^{\rm sing}(t) + \phi_{\mathbf{V}}^{(D)}(t)\,. \tag{31}$$

The first term on the right-hand side of (31) is of a singular character and is described by the expression [29]

$$\phi_{\mathbf{V}}^{\rm sing}(t) = \frac{2k_{\rm B}T}{m_{\rm L}}\exp(-x)P(x)\theta\left(\frac{2}{\kappa - x}\right), \tag{32}$$

$$P(x) = \left[1 + \frac{1}{2}(2-3\kappa)\,x + \frac{1}{4}(2-3\kappa)x^2 - \frac{\kappa}{8}(3-2\kappa^2)x^3 + \frac{1}{16}\kappa^3 x^4 + \frac{1}{32}\kappa^3 x^5\right], \tag{33}$$

where $x = t/(2\tau_{\rm M})$,

$$\theta(x) = \begin{cases} 1, & x \geqslant 0, \\ 0, & x < 0\,, \end{cases}$$

is the Heaviside function, and $\kappa = 4v\tau_{\rm M}/r_{\rm L}^2$. When using the estimate $r_{\rm L} = r_*, r_* = 2\sqrt{v\tau_{\rm M}}$ defining the collective contribution to the self-diffusion coefficient, $\kappa = 1$.

The second term on the right-hand side of (31) is described by the expression [71]

$$\phi_{\mathbf{V}}^{(D)}(t) = \frac{2D_{\rm c}^{(F)}}{\tau_{\rm M}}\frac{\exp(-x)}{x}\big(I_1(x) + I_2(x)\big)\theta(x-1)\,, \tag{34}$$

where $D_{\rm c}^{(F)} = k_{\rm B}T/(8\pi\eta r_{\rm L})$, and $I_n(x)$, $n = 1, 2$ denote the Bessel functions of the imaginary argument. If $x \gg 1$, the function $\phi_{\mathbf{V}}^{(D)}(t)$ has the following asymptotic form:

$$\phi_{\mathbf{V}}^{(D)}(t) = \frac{A}{t^{3/2}}\left(1 - \frac{9}{4}\frac{\tau_{\rm M}}{t} + \ldots\right), \tag{35}$$

whose leading term coincides with (1) and (2).

The component $\phi_{\mathbf{V}}^{\rm P}(t)$ is governed by thermal and sound modes, and the latter dominate. If the thermal modes are ignored, this component can be approximated by the expression [29]

$$\phi_{\rm s}^{\rm l}(x) = \frac{3}{\pi}\frac{k_{\rm B}T}{m_{\rm L}}\int_0^\infty \frac{{\rm d}u}{u^2}\left(\cos u - \frac{\sin u}{u}\right)^2 \times \exp\left(-\sigma u^2\frac{t}{r_{\rm L}^2}\right)\cos\left(c_{\rm l}\frac{u}{r_{\rm L}}t\right), \tag{36}$$

where $c_{\rm l}$ is the longitudinal sound speed, $\sigma = (1/2)\times[\nu + \lambda(\gamma - 1)]$ is the coefficient of sound decay, $\lambda = \chi/(\rho C_p)$, χ is the heat conductivity coefficient, $\gamma = C_p/C_v$, and C_p and C_v are the isobaric and isochoric specific heats.

The spectral density of a VACFM is given by the expression

$$\phi_{\mathbf{V}}(\omega) = \frac{1}{\pi}\int_0^\infty \phi_{\mathbf{V}}(t)\cos(\omega t)\,{\rm d}t\,,$$

and in accordance with (29) and (30) has the following structure:

$$\phi_{\mathbf{V}}(\omega) = \phi_{\mathbf{V}}^{\rm M}(\omega) + \phi_{\mathbf{V}}^{\rm S}(\omega) + \phi_{\mathbf{V}}^{\rm P}(\omega)\,. \tag{37}$$

The behavior of the second and third terms is studied in detail in Refs [29, 40], where, in particular, it is shown that the spectral density of $\phi_{\mathbf{V}}^{(D)}(t)$ is given by the expression

$$\phi_{\mathbf{V}}^{(D)}(\omega) = 2D_{\rm c}^{(F)}{\rm Re}\left[-\frac{1}{2} + b(1+b) - (1+b)\sqrt{b^2-1}\right], \quad b = 1 - {\rm i}z\,, \quad z = 2\omega\tau_{\rm M}\,, \tag{38}$$

which leads to the following low-frequency asymptotic form:

$$\phi_{\mathbf{V}}^{(D)}(\omega) = 3D_{\rm c}^{(F)}\left[1 - \frac{4}{3}\sqrt{2\pi\omega\tau_{\rm M}} \times \left(1 - \frac{3}{2}\omega\tau_{\rm M} + \frac{3}{8}(\omega\tau_{\rm M})^2\right) + \ldots\right], \quad \omega\tau_{\rm M} \ll 1\,. \tag{39}$$

Its most prominent feature is the square root character of the dependence on frequency, which is a reflection of vortical

motions in liquids. A similar dependence was discovered in the recent study [72], where the spectrum of the VACFM was studied experimentally with the help of the spin echo method. However, this method detects only relatively large-scale vortices, with lifetimes of $\sim 10^{-4}$ s.

Details of the behavior of $\phi_{\mathbf{V}}^{(D)}(\omega)$ and $\phi_{\mathbf{V}}^{\mathrm{H}}(\omega)$ are described in Ref. [56].

4. Maxwell relaxation time for argon and water determined with the help of computer modeling

In this section, the main focus is on finding temperature dependences of the MRT for liquid water and argon on their existence curves, as well as discussing limiting temperatures for their potential applications.

4.1 General requirements for the Maxwell relaxation time

By definition (for details, see Refs [50, 73, 74]), the MRT of a liquid is linked to its dynamical shear viscosity η and high-frequency shear modulus G_∞ through a relation like (16), $\tau_{\mathrm{M}} = \eta/G_\infty$. Taking into account that $\eta = \rho v$ and $G_\infty/\rho = c_{\mathrm{t}}^2$, where c_{t} is the transverse sound speed at high frequencies, for MTR we find

$$\tau_{\mathrm{M}} = \frac{v}{c_{\mathrm{t}}^2}\,. \tag{40}$$

Because the transverse c_{t} and longitudinal c_{l} speeds satisfy the inequality $c_{\mathrm{t}} < c_{\mathrm{l}}$ for high-frequency sound, we arrive at the following limitation imposed on the MRT:

$$\tau_{\mathrm{M}} > \tau_{\mathrm{M}}^{\mathrm{l}}\,, \quad \tau_{\mathrm{M}}^{\mathrm{l}} = \frac{v}{c_{\mathrm{l}}^2}\,. \tag{41}$$

Numerical values of $\tau_{\mathrm{M}}^{\mathrm{l}}$ (which correspond to the values of c_{l} at several temperatures [75–77]), as well as data for τ_{M} known from the literature, are listed in Table 1. Somewhat unexpectedly, the MRT values given in the literature, except for those of Ref. [74], violate inequality (41). As concerns the values from Ref. [74], they are obtained through a method that is not fully justified.

The second inequality relies on the requirement that the appropriate radius of a Lagrangian particle be bounded from below. It cannot be smaller than the size of the molecular complex formed by the molecule and its nearest neighborhood, i.e.,

$$\zeta > 1\,, \quad \zeta(T) = \frac{2\sqrt{v(T)\tau_{\mathrm{M}}(T)}}{3r_{\mathrm{p}}}\,, \tag{42}$$

because, otherwise, the hydrodynamic size will be smaller than the molecular one. Temperature T_*, satisfying the equation

$$\zeta(T_*) = 1\,, \tag{43}$$

bounds from above the MRT applicability region. For larger temperatures, hydrodynamic modes in the system will be diffusive, and the values of the VACFM will be positive at all times or only slightly enter the negative domain. In this case, the notion of a Lagrangian particle loses its meaning, and the thermal drift of molecules loses its collective component.

Table 1. Values of τ_{M} and $\tau_{\mathrm{M}}^{\mathrm{l}}$ for liquid argon on its existence curve.

T, K	τ_{M}, 10^{-13} s [50]	τ_{M}, 10^{-13} s [73]	τ_{M}, 10^{-13} s [74]	$\tau_{\mathrm{M}}^{\mathrm{l}}$, 10^{-13} s
90	≈ 2.28	1.68	—	2.68
100	—	—	—	2.51
110	—	1.58	≈ 21	2.45
120	—	1.57	≈ 22	2.75
130	—	1.66	—	3.3
140	—	1.73	—	4.85
150	—	—	—	—

4.2 Finding the Maxwell relaxation time for water

Low-frequency VACF spectra possess the simplest structure if temperatures are sufficiently high. In this case, they are defined largely by diffusive vortical modes of the molecular velocity field. As an example, the structure of the VACF spectrum is presented in Fig. 2 for $T = 550$ K.

At temperature $T = 274$ K (Fig. 3) the low-frequency VACF spectrum can be only unsatisfactorily reproduced with the help of (39). This circumstance arises because the behavior of the spectrum in this case is governed by both transverse and longitudinal modes. In all probability, modeling the latter by only acoustical contributions like (36) is insufficiently fine. Fortunately, here, to determine the MRT, it is sufficient to achieve a satisfactory reproduction of the lowest-frequency raising interval in the VACF spectrum.

The values of the MRT obtained by an optimal fit of model spectral curves to the formula $\phi_{\mathbf{V}}(\omega) = \phi_{\mathbf{V}}^{\mathrm{S}}(\omega) + \phi_{\mathbf{V}}^{\mathrm{P}}(\omega) + \ldots$, where $\phi_{\mathbf{V}}^{\mathrm{S}}(\omega)$ is given by the sum $\phi_{\mathbf{V}}^{\mathrm{sing}}(\omega)$ (spawned by (32))

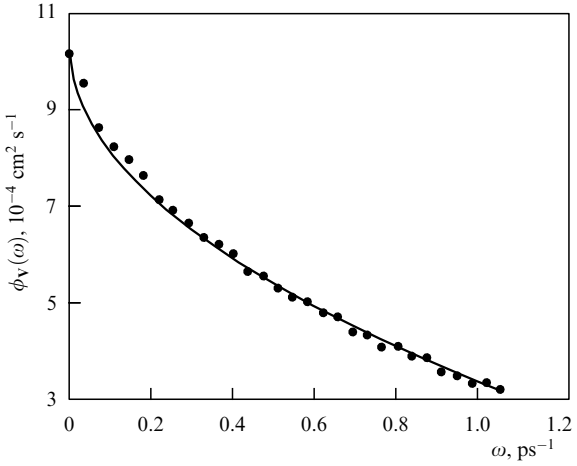

Figure 2. Character of the fit for the low-frequency component in the spectrum of the VACF of water performed with the help of expansion (39) at $T = 550$ K.

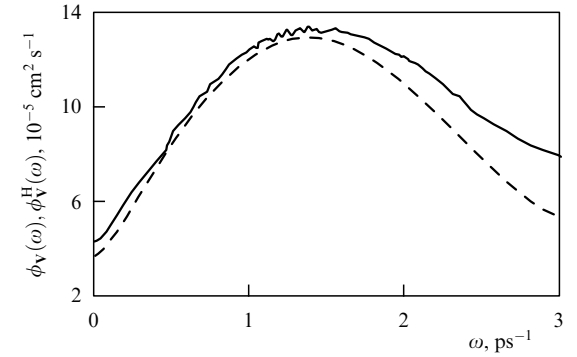

Figure 3. Optimal fit of VACF low-frequency model spectrum (solid line) with the help of $\phi_{\mathbf{V}}^{\mathrm{H}}(\omega)$ that correspond to $\phi_{\mathbf{V}}^{\mathrm{H}}(t) = \phi_{\mathbf{V}}^{\mathrm{sing}}(t) + \phi_{\mathbf{V}}^{(D)}(t) + \phi_{\mathbf{V}}^{\mathrm{P}}(t)$, where the behavior of the components is defined by formulas (32), (34), and (36) for $T = 274$ K (dashed line).

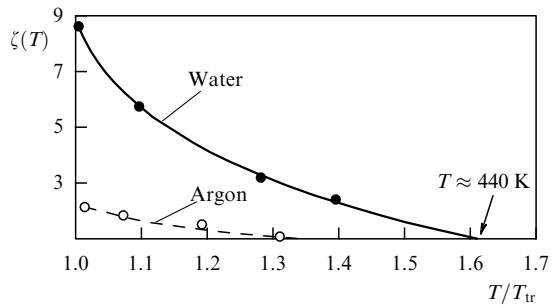

Figure 4. Temperature dependences $\zeta(T)$ for water and argon. T_{tr} is the respective triple point temperature.

Table 2. Temperature dependence of τ_M, D_c, and D_s for water.

T, K	τ_M, ps	D_s^{MD}, 10^{-5} cm^2 s^{-1}	D_s^{exp}, 10^{-5} cm^2 s^{-1} [78, 79]	D_c, 10^{-5} cm^2 s^{-1}	D_c/D_s
274	0.98	1.529	1.18	0.053	0.045
300	0.866	2.779	2.41	0.179	0.074
350	0.612	7.04	6.28	0.866	0.138
380	0.489	11.07	9.33	1.732	0.186

and $\phi_V^{(D)}(\omega)$ (38), and the spectrum $\phi_V^P(\omega)$ is given by the expression $\phi_s^1(x)$ (36), are collected in Table 2.

These data need to be complemented by a consideration of the temperature dependence of parameter $\zeta(T)$ which defines the region where transverse elastic oscillations can be manifested in the VACF spectra for water molecules. As can be seen from Fig. 4, this parameter tends to unity for $T \approx 440$ K. This value of temperature proves to be close to another characteristic temperature, $T_F \approx 400$ K, which corresponds to the disappearance of the plateau region in the behavior of function $F_{MD}(x)$. Furthermore, it is also close to the temperature $T \approx 420$ K at which the interval of negative values in the VACF of water molecules disappears.

The values of the MRT for water can be formally determined at higher temperatures as well. However, in this case, inequalities (41) and (42) are violated (either one of them or both), and the MRT loses its meaning. In other words, the reaction of the system to low-frequency external perturbations remains viscid, and transverse modes preserve their diffusive character.

4.3 Maxwell relaxation time for argon

In the case of argon, the MRT and other quantities discussed by us are defined similarly. They are all presented in Table 3.

Table 3. Values of τ_M, D_s, and D_c/D_s for argon for several temperatures.

T, K	τ_M, ps	D_s^{MD}, 10^{-5} cm^2 s^{-1}	D_s^{exp}, 10^{-5} cm^2 s^{-1} [80 – 82]	D_c, 10^{-5} cm^2 s^{-1}	D_c/D_s
85	0.838	1.91	2.07	0.305	0.147
90	0.682	2.31	2.36	0.456	0.193
100	0.655	3.41	3.52	0.788	0.223

Table 4. Ratios D_c/D_s for argon obtained by the values of the characteristic function and computed directly.

T, K	$F_{MD}(x)$ (27)	D_c/D_s (13)
85	0.138	0.159
90	0.151	0.197
100	0.182	0.231

From Table 4 and the dependence $\zeta(T)$ (see (42)), it follows that the characteristic temperature T_F^{Ar} proves to be close to 110 K.

5. Manifestation of collective drift in the mean quadratic displacement of molecules

In this section, we consider a direct manifestation of collective drift in the MSD of molecules of liquid argon and water, determined with the help of computer modeling, and also estimate the ratio D_c/D_s for these substances.

5.1 Mean square displacement of molecules of argon and water

The behavior of dimensionless MSD $\tilde{\Gamma}_{MD}(x)$ for molecules of argon and water, as well as the characteristic function $F_{MD}(x)$, which differs from zero only if there is a collective drift of molecules, is depicted in Fig. 5. As follows from Fig. 5, there is no visually discernible manifestation of the square-root contribution in the MSD of molecules. At the same time, if we turn to the characteristic function $F_{MD}(x)$, the fact that it exists becomes trivial. Note that widening of curves $\tilde{\Gamma}_{MD}(x)$ and $F_{MD}(x)$ is noticeable only beyond x_u.

5.2 Finding the relative value of the collective component of the self-diffusion coefficient in argon and water

The dependence of characteristic function $F_{MD}(x)$ on x, averaged over six motion trajectories of molecule in the interval $x_l < x < x_u$, where the lower bound satisfies the inequality $x_l > 1$, is plotted in Fig. 6.

We need to note that the plateau in the behavior of characteristic function $F_{MD}(x)$ is formed only at temperatures $T < 120$ K, i.e., there is no collective transport at higher temperatures. At such temperatures, the size of a Lagrangian particle with the appropriate radius approaches the size of a single molecule, which does not make sense (as mentioned in Section 4.1). The values of D_c/D_s for argon, found from an analysis of the behavior of characteristic function $F_{MD}(x)$, are placed in the second column of Table 4. The third column of this table gives the values of D_c/D_s, where D_c is computed by formula (13) and for D_s its experimental values are taken [80–82].

As can be seen, the collective component D_c in the self-diffusion coefficient amounts to approximately 14–16% of its total value in the vicinity of the argon triple point and increases to 19–26% on approaching $T_* \approx 120$ K. In the vicinity of this temperature, D_c drops to zero, which can be described by approximating the MRT using the formula

$$\tau_M(T) = \tau_M^{MD}(T)\frac{1}{2}\left\{1 - \tanh\left[\gamma(T - T_*)\right]\right\},$$

where $\gamma|T - T_*| \ll 1$ only in a small vicinity of point T_*. It is assumed that $\tau_M^{MD}(T)$ can be found for all temperatures of the liquid state.

The consideration for water is identical and leads to the results presented in Table 5.

5.3 Indicator of the existence of collective transport in liquids

The analysis of the magnitude and temperature dependence of the self-diffusion coefficient of a molecule helps to propose one more indicator of the existence of collective transport in liquids. This analysis rests on a comparison of temperature dependences of effective radii of molecules found studying

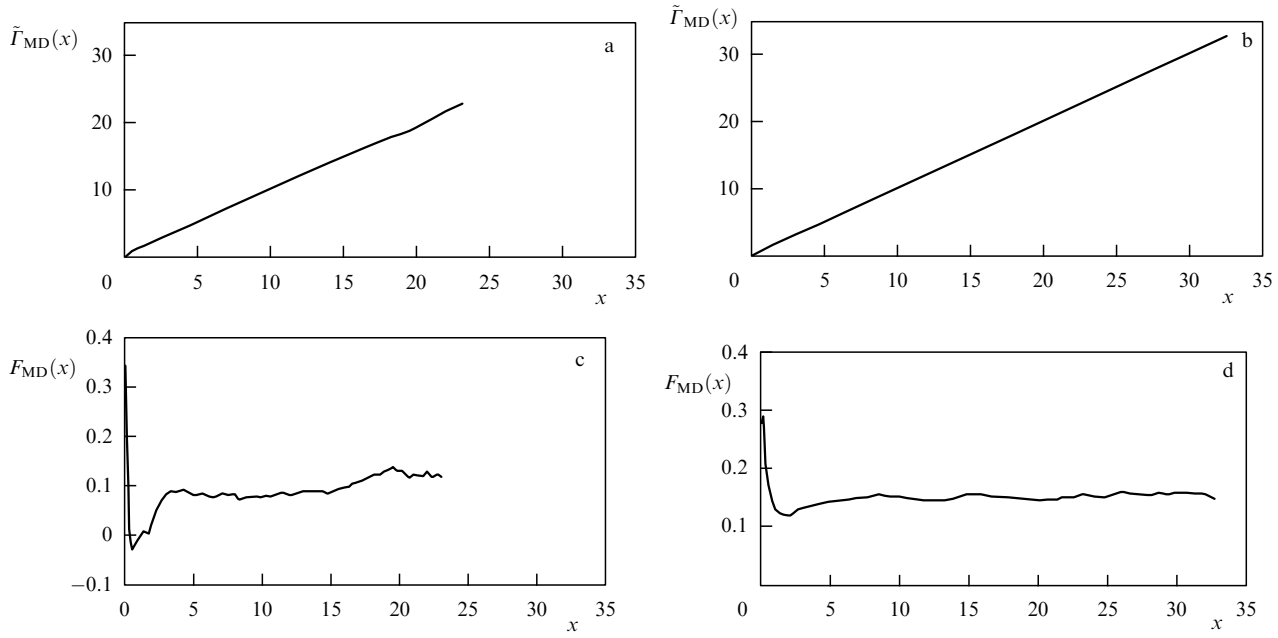

Figure 5. Dependence of $\tilde{\Gamma}_{\rm MD}(x)$ and $F_{\rm MD}(x)$ on the dimensionless time x for water (a, c) and argon (b, d).

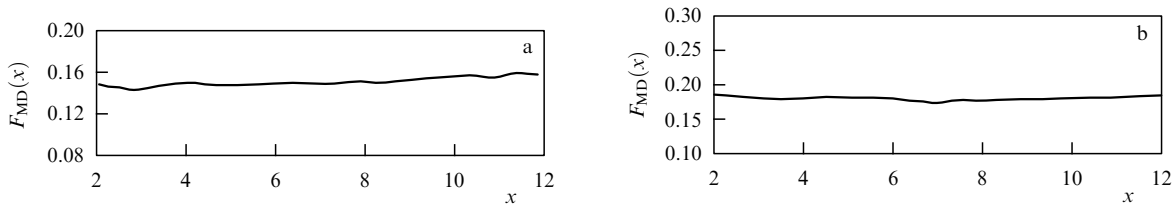

Figure 6. Behavior of $F_{\rm MD}(x)$ for argon at $x_{\rm l} < x < x_{\rm u}$ for temperatures $T = 85$ K (a) and $T = 100$ K (b).

Table 5. Values of $D_{\rm c}/D_{\rm s}$ for several temperatures for water. *

T, K	$D_{\rm s}^{\rm MD}$	$D_{\rm s}^{\rm exp}$	$F_{\rm MD}(x)$ (27)	$D_{\rm c}/D_{\rm s}$ (13)
274	1.529	1.18	0.022	0.05
300	2.779	2.41	0.081	0.089
350	7.04	6.28	0.157	0.143
380	11.07	9.33	0.243	0.191

* The experimental values are taken from Refs [75, 76].

temperature dependences of their self-diffusion coefficients in the absence and presence of collective drift. Indeed, fitting the Einstein formula to the experimental data for the self-diffusion coefficient, we get the following expression for the effective radius of a molecule of liquid:

$$r_D(T) = \frac{k_{\rm B}T}{6\pi\eta(T)D_{\rm s}(T)}\,. \tag{44}$$

On the other hand, based on our knowledge, the value of the self-diffusion coefficient is the sum of two collective components that correspond to contributions from the nanoscopic and molecular modes:

$$D_{\rm s}(T) = \frac{k_{\rm B}T}{6\pi\eta(T)}\left(\frac{1}{r_{\rm p}} + \frac{6}{5}\,\frac{1}{r_*(T)}\right).$$

Hence, it follows that

$$\frac{1}{r_{\rm eff}(T)} = \frac{1}{r_{\rm p}} + \frac{6}{5}\,\frac{1}{r_*(T)}\,, \tag{45}$$

where $r_{\rm p}$ is assumed to be independent of temperature and equal to the value that follows from the analysis of kinematic shear viscosity in liquids [49, 83]. Our views on the character of self-diffusion will correspond to experimental data if the relationship

$$\frac{r_{\rm eff}(T)}{r_D(T)} \approx 1 \tag{46}$$

is observed in the whole interval of liquid states, or, more precisely, its deviation from unity is within experimental error. Formula (46) can be written in the following equivalent form:

$$\frac{r_D(T)}{r_{\rm p}} = \begin{cases} 1 - \dfrac{2}{5\zeta(T)+2}\,, & T_{\rm tr} < T < T_*\,, \\ 1\,, & T_* < T\,. \end{cases} \tag{47}$$

For $T \to T_*$ $\zeta(T) \to 1$; hence,

$$\left.\frac{r_D(T)}{r_{\rm p}}\right|_{T\to T_*} \to \frac{5}{7}\,. \tag{48}$$

The correspondence of relationships (47) and (48) to experimental data for argon and water is illustrated in Fig. 7.

As can be seen, agreement between experimental and computational data in temperature intervals $T_{\rm tr} < T < T_*$ for argon and water is practically complete. The inequality $r_D(T)/r_{\rm p} \approx 1$ for $T_* < T$ is fulfilled with the same degree of accuracy.

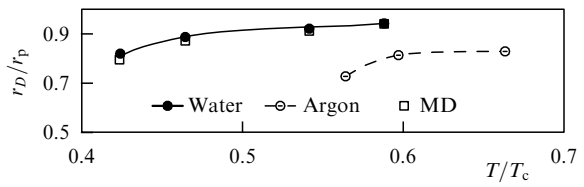

Figure 7. Temperature dependences of the ratios of the molecule diffusive radius to its kinetic radius ($r_D(T)/r_p$) for argon and water: the curves correspond to formula (47) and symbols correspond to experimental data. We used $r_p^{Ar} = 1.41$ Å [83] and $r_p^{H_2O} = 1.2$ Å [84].

6. Some features of the behavior of the velocity autocorrelation function for molecules of water and argon

The VACF of argon and water molecules has been the subject of numerous modeling studies relying on MD methods [5–8, 85–89]. This is why we limit ourselves in this section to presenting 1) details pertaining to the behavior of the VACF of argon molecules on approaching the binodal and spinodal points, as well as at large separation from them; 2) differences in VACF behavior for water and argon molecules. All details of VACF behavior will be presented as functions of temperature and density, which can be rewritten as functions of pressure by resorting to the system equation of state.

Direct reconstruction of the VACFM as a function of pressure is also possible with the help of an *NPT*-ensemble. However, in this case, modeling of overcooled states would present difficulties.

One may consult Appendix 1 for details about the MD experiment and VACF reconstruction procedure for liquid argon and water molecules.

6.1 Velocity autocorrelation function of argon molecules in the vicinity of or far from the spinodal and binodal

The spinodal of a system is its important thermodynamical characteristic separating the regions of stable and metastable states from the region of absolutely unstable states. The position of the spinodal for argon was determined by various methods in Refs [90–92] (Fig. 8).

It seems natural to assume that the transition to the region of absolutely unstable states would be accompanied by a noticeable change in the behavior of the VACF of molecules. This assumption is indeed confirmed by the results of MD modeling presented in Figs 9 and 10.

Attention is drawn to the fact that the decay of the VACF of an argon molecule on isochore $\rho = 0.9$ g cm^{-3} becomes nonnegative at $T \approx 95$ K (i.e., the VACF ceases to take negative values), and for $T \approx 130$ K it becomes monotone. Temperature $T \approx 130$ K corresponds to the point where the spinodal is intersected by the isochore [75, 90], i.e., all other temperatures that were considered are in the domain located under the spinodal.

Note that in the region of absolutely unstable states, i.e., under the spinodal, the distribution of particles in the volume of the computational cell becomes inhomogeneous; however, the position of void regions is not fixed and no irreversible partitioning into liquid and gas takes place.

From our consideration, it follows that the larger the system density, the more expressed is the appearance of the region of negative values in the VACFM. Yet neither the argon liquid–gas coexistence curve nor its spinodal are directly seen in the VACF behavior. In Section 7.2, it is shown that this happens given spontaneous symmetry violation in the model system.

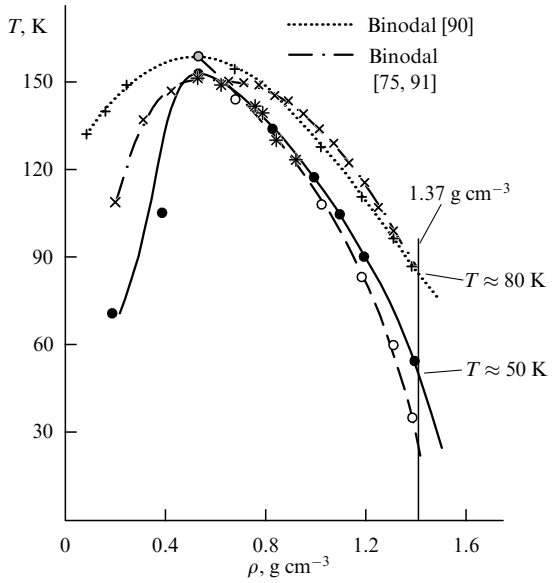

Figure 8. Spinodal and binodal of argon: the position of the binodal is marked by the dotted curve (according to Ref. [90]) and dashed-dotted curve (according to Refs [75, 91]). The position of the spinodal is shown by the dashed curve [90]. Stars correspond to experimental data from Ref. [91]. The black dots depict the results of computations in Ref. [92]; the solid line is the argon spinodal as the result of interpolation of data obtained in Ref. [92].

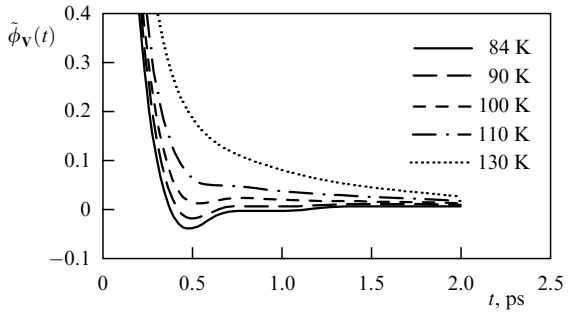

Figure 9. Behavior of the VACF of an argon molecule on the isochore $\rho = 0.9$ g cm^{-3} at different temperatures.

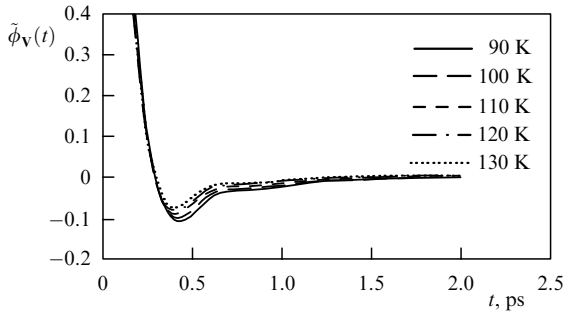

Figure 10. Behavior of the VACF of an argon molecule on the isochore $\rho = 1.41$ g cm^{-3} at different temperatures.

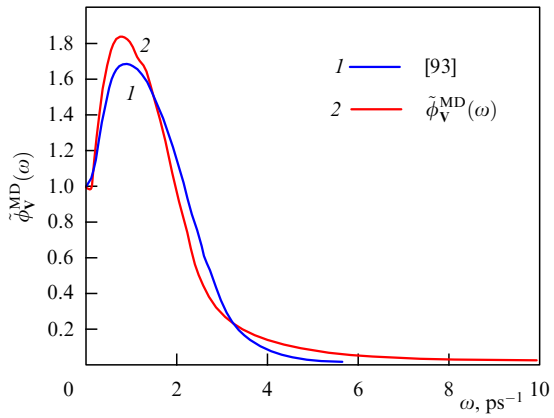

Figure 11. (Color online.) Behavior of spectral densities of the VACF of argon molecules $\tilde{\phi}_{\mathbf{V}}(\omega) = \phi_{\mathbf{V}}(\omega)/\tilde{\phi}_{\mathbf{V}}(0)$ for $T = 183$ K and $\rho = 1.6$ g cm^{-3}; the blue line corresponds to the results of Ref. [93], the red one corresponds to our MD computations (*NVE*-ensemble, 64,000 particles).

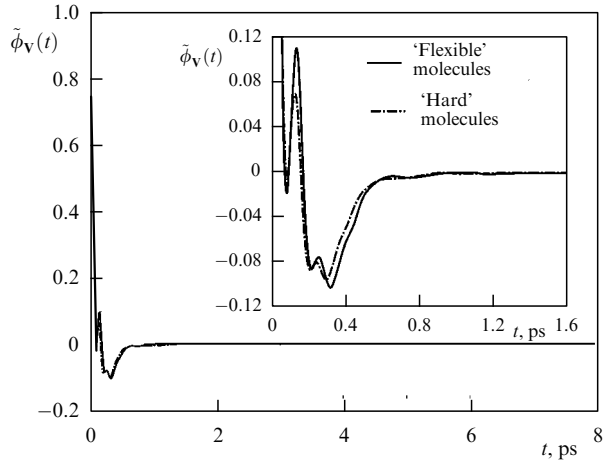

Figure 12. Behavior of the VACF of water molecules for $T = 274$ K using different plotting scales.

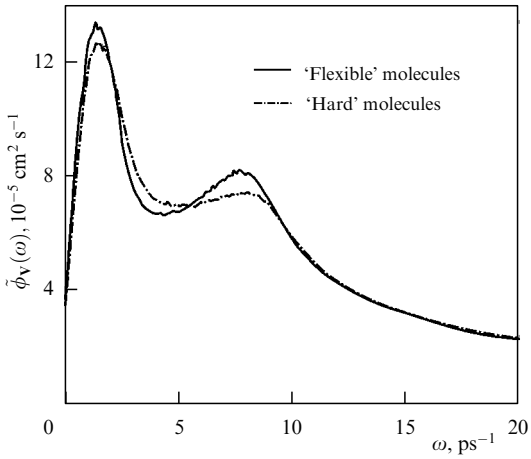

Figure 13. Details of the spectrum of the VACF of water molecules for $T = 274$ K.

6.2 Spectral density of velocity autocorrelation function of the argon molecule

The general structure of spectral density $\phi_{\mathbf{V}}(\omega)$ is depicted in Fig. 11, which also presents an analogous dependence from Ref. [93], which studied the VACFM based on quasiclassical modeling of the dynamics of liquid argon molecules. The comparison demonstrates rather satisfactory agreement between the spectral densities of the VACFM, and the frequencies of VACF spectral maxima practically coincide.

The collective contributions in the VACF of argon molecules are noticeable in their spectra only in the low-frequency region ($\omega \ll (<) 1/\tau_{\mathrm{M}}$), where they are described by the universal asymptotic form (39). The spectral density maximum occurring at $\tilde{\omega}_* \approx 0.1$ is observed at temperatures close to the argon triple point. At sufficient separation from the triple point, the transverse modes become diffusive, while longitudinal modes become strongly decaying, and the low-frequency peak in the VACF spectrum of argon molecules disappears.

6.3 Velocity autocorrelation function of water molecules and its spectral density

The behavior of the VACF of water molecules as a whole is the same as for argon, yet differs in some important details. In the region where the VACF of water molecule is at a minimum, as can be seen from Fig. 12, a fine structure (FS) is formed owing to the effects of dimerization. The most robust details of the FS are practically insensitive to the choice of hard or soft intermolecular potentials, i.e., those potentials that take or do not take into account possible changes in the configuration of water molecules.

The low-frequency component of the spectral density of the VACF of water molecules that is related to the TC (see the insert in Fig. 12) is plotted in Fig. 13. Here, the rather strong low-frequency peak centered around $\omega_{\mathrm{p}} \sim 1.5$ ps^{-1} comes from the contributions of elastic transverse and longitudinal modes. A weaker and less confined peak close to $\omega_{\mathrm{d}} \approx 7$ ps^{-1} corresponds to thermal oscillations of dimers.

The low-frequency peak is observed for supercooled water states and for normal water states if the temperature is bounded from above, $T_{\mathrm{tr}} < T < T_*$.

The value of T_* is estimated from the equation

$$\tilde{\phi}_{\min}(T_*) \approx 0.1\tilde{\phi}_{\min}(T_{\mathrm{tr}})$$

and is $T_* \approx 400$ K. For higher temperatures, the reaction of the system to external perturbations remains viscous even at frequencies $\omega > 1/\tau_{\mathrm{M}}$.

On a qualitative level, similar limitations also pertain to the weaker peak which appears due to dimerization effects and is observed only for $T < T_{\mathrm{d}}$, with T_{d} being estimated in Appendix 2 as $T_{\mathrm{d}} \approx 450$ K.

6.4 High-frequency asymptotic form of the velocity autocorrelation function of argon and water molecules

Also very revealing is the high-frequency asymptotic form of the VACFM [94, 95], which also possesses a universal exponential character (Fig. 14):

$$\phi_{\mathbf{V}}(\omega)\big|_{\omega\to\infty} \sim A_m\big(\omega\tau_{\mathrm{a}}(m)\big)^{q(m)} \exp\Big[-\big(\omega\tau_{\mathrm{a}}(m)\big)^{p(m)}\Big], \quad (49)$$

where the coefficient A_m, the power-law indices $p(m)$ and $q(m)$, and the characteristic time $\tau_{\mathrm{a}}(m)$ of spectral density

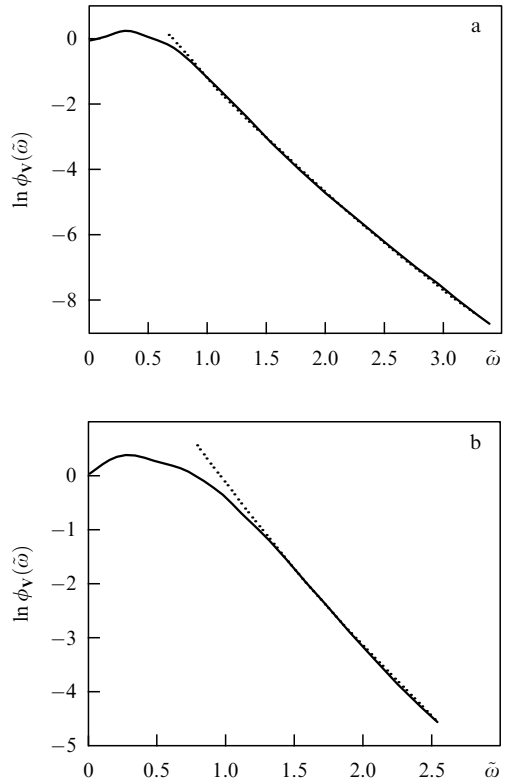

Figure 14. High-frequency asymptotic form of the VACF spectra of argon molecules that correspond to various values of the power-law index in the repulsion potential: (a) $m=12$, (b) $m=18$. The dotted lines plot the result of computations based on (49). Here, $\tilde{\omega}=\omega h/(k_{\mathrm{B}}T)$, where h is the Planck constant, $T=94.4$ K.

decay are certain functions of the power-law index m of the repulsion potential

$$U_{\mathrm{R}}(r)=\varepsilon\left(\frac{\sigma}{r}\right)^{m}.$$

References [94, 95] show that $p(m)$ and $q(m)$ are given by the following expressions:

$$p(m)=\frac{2m}{3m+2}\,,\quad q(m)=\frac{1}{3}-2\left(\frac{7}{9m+6}+\frac{2}{m+2}\right).$$

The characteristic time $\tau_{\mathrm{a}}(m)$ has the sense of the duration of a hard collision between two molecules.

The pertinence of formula (49) for spectral density, constructed by MD modeling methods for the potentials

$$U(r)=\varepsilon\left[\left(\frac{\sigma}{r}\right)^{m}-\left(\frac{\sigma}{r}\right)^{6}\right],$$

is illustrated in detail in Ref. [95]. There is practically no expression of attraction forces in high-frequency spectra of the VACFM. The deviation of m from 12 in a wide range of temperatures and pressures is discussed, in particular, in Refs [96–100].

In this respect, the process of collisions between molecules in liquids can be viewed as a composition of 1) sequential hard collisions between pairs of molecules and 2) soft collisions of a multiparticle nature caused mainly by attraction forces. The duration of this collisional component is characterized by the time

$$\tau_{\mathrm{s}}\sim\frac{\sigma}{V_T}\sim 10^{-12}\ \mathrm{s}\,.$$

The hard component of collisions is present only if there is direct contact between molecules, which has, as a rule, a pair character, and its duration τ_{h} turns out to be much shorter than τ_{s} (see [95]):

$$\tau_{\mathrm{h}}\sim\frac{1}{m}\tau_{\mathrm{s}}\,.$$

The notions of hard and soft collisions in liquids are also used in Refs [101, 102] when constructing the Rice–Allnatt kinetic equation. Namely these components of collisions define the high-frequency asymptotic form of not only the VACF spectra but also other correlation functions.

It is noteworthy that the analysis of high-frequency spectra for molecular light scattering is the most straightforward method of finding the repulsion power-law index m [94, 95, 103–105].

7. Finding self-diffusion and shear viscosity coefficients in liquids

The adequacy of modeling the VACF using molecular dynamics methods is attested to by comparing the values for the coefficients of self-diffusion D_{s} and shear viscosity v with experimental data.

7.1 Coefficients of self-diffusion and shear viscosity

The self-diffusion coefficient is defined by the equation

$$D_{\mathrm{s}}^{(\phi)}=\frac{1}{3}\int_0^{\infty}\phi_{\mathbf{V}}^{\mathrm{MD}}(t)\,\mathrm{d}t \tag{50}$$

or the relationship

$$D_{\mathrm{s}}^{(\Gamma)}=\left(\frac{\Gamma^{\mathrm{MD}}(t)}{6t}\right)\Big|_{t\to\infty}, \tag{51}$$

where $\phi_{\mathbf{V}}^{\mathrm{MD}}(t)$ and $\Gamma^{\mathrm{MD}}(t)$ are the values of the VACF and mean square displacement for a molecule found in computer simulations. It is supposed that the degree to which the thus found coefficients of self-diffusion agree between themselves and with the related experimental data,

$$D_{\mathrm{s}}^{(\phi)}\,,\quad D_{\mathrm{s}}^{(\Gamma)}\approx D_{\mathrm{s}}^{\mathrm{exp}}\,,$$

is one of the crucial factors in favor of the correctness of the method used by us to compute them.

The value of shear viscosity v can be found from the long-term asymptotic form of the VACFM,

$$\phi_{\mathbf{V}}^{\mathrm{MD}}(t)\big|_{t\to\infty}=\frac{A_{\mathrm{t}}^{\mathrm{MD}}}{t^{2/3}}+\ldots\,,$$

with the coefficient A given by relationship (2). It follows that

$$v_{\mathrm{t}}^{\mathrm{MD}}=\frac{1}{\pi}\left(\frac{k_{\mathrm{B}}T}{4\rho A_{\mathrm{t}}^{\mathrm{MD}}}\right)^{2/3}. \tag{52}$$

A more advantageous approach, however, lies in determining shear viscosity from the explicit form of the low-frequency asymptotic form of the VACF spectral density.

Table 6. Values of self-diffusion coefficient of argon molecules computed by formulas (50) and (51).

T, K	$\rho_{\mathrm{Ar}}^{\mathrm{exp}}$, g cm^{-3}	$D_{\mathrm{Ar}}^{\mathrm{exp}}$, 10^{-5} cm^2 s^{-1}	$D_{\mathrm{Ar}}^{\mathrm{MD}}$, 10^{-5} cm^2 s^{-1} (50)	$D_{\mathrm{Ar}}^{\mathrm{MD}}$, 10^{-5} cm^2 s^{-1} (51)
90	1.379	2.36	2.31	2.304
100	1.314	3.52	3.62	3.59
110	1.243	4.85	4.72	4.79
120	1.163	6.02	6.11	6.065
130	1.068	7.43	7.44	7.48
140	0.944	8.82	8.95	9.01
150	0.68	—	12.37	12.45

Table 7. Values of kinematic shear viscosity of argon computed by formula (54).

T, K	v_ω^{MD}, 10^{-3} cm^2 s^{-1}	v_{exp}, 10^{-3} cm^2 s^{-1} [75]	ε_v
90	3.2	1.903	0.71
100	2.1	1.4	0.5
110	1.46	1.1	0.33
120	0.964	0.937	0.21
130	0.88	0.878	0.13
140	0.674	0.648	0.09
150	—	0.519	—

This is explained by the fact that random short-period pulsations of the temporal dependence in the region of the VACF power-law tail are cut off by the Fourier transform at low frequencies. Taking into account that $\phi_{\mathbf{V}}(\omega = 0) = 3D_{\mathrm{s}}$, and also that the main contribution in the spectral density of the VACFM to the lowest frequencies comes from the vortical modes, we find

$$\phi_{\mathbf{V}}(\omega)\big|_{\omega\to 0} = 3D_{\mathrm{s}} - B\sqrt{\omega} + \ldots , \tag{53}$$

where the coefficient B is defined by the values of low-frequency spectral density $\phi_{\mathbf{V}}^{\mathrm{MD}}(\omega)$. Then,

$$v_\omega^{\mathrm{MD}} = \frac{1}{\pi}\left(\frac{k_{\mathrm{B}}T}{4\rho A_\omega^{\mathrm{MD}}}\right)^{2/3}, \tag{54}$$

where $A_\omega^{\mathrm{MD}} = B/(2^{1/2}\pi)$. The validity of the relationship

$$v_{\mathrm{t}}^{\mathrm{MD}}, \quad v_\omega^{\mathrm{MD}} \approx v_{\mathrm{exp}}$$

is the second important indicator of the correctness of our computations.

Numerical values of the self-diffusion and shear viscosity coefficients computed by formulas (50), (51), and (54) respectively, are listed in Tables 6 and 7.

As can be seen, the agreement between the computed and experimental data for argon is highly satisfactory. The closeness of the values of v_ω^{MD} and v_{exp} explicitly attests to the hydrodynamic nature of the power-law tail of the VACFM.

In the case of water (Table 8), the agreement between our computations and experimental values is notably worse, which in all probability is related to the fact that long-time tails of the VACFM are prominent enough only at times t in excess of the dynamical memory time t_{d} of MD computations.

Table 8. Values of kinematic shear viscosity of water computed by formula (54).

T, K	v_ω, 10^{-3} cm^2 s^{-1}	v_{exp}, 10^{-3} cm^2 s^{-1} [75]	ε_v
274	13.7	17.4	0.21
300	7.61	8.53	0.2
350	3.41	3.8	0.1
380	2.6	2.8	0.06
450	—	—	—
480	1.2	1.51	0.22
550	1.3	1.253	0.02

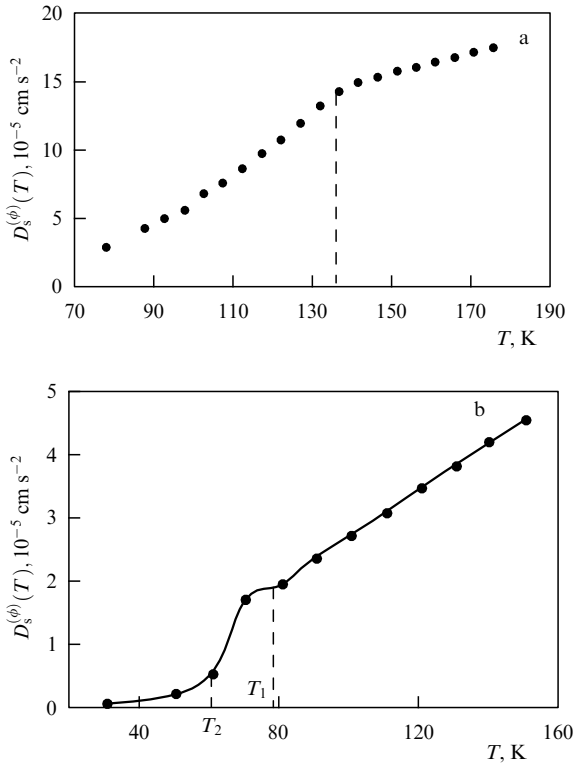

Figure 15. Temperature dependence of self-diffusion coefficient of argon on the isochores $\rho = 0.837$ g cm^{-3} (a) and $\rho = 1.37$ g cm^{-3} (b).

7.2 Locations of spinodals and binodals of argon and water

There is one surprising feature intrinsic to the temperature dependences of profiles of the VACFM on isochores: the related self-diffusion coefficients $D_{\mathrm{s}}^{(\phi)}(T)$, considered as functions of temperature on different isochores, change their slope at spinodal and binodal points. This effect is most apparent at spinodal points (Fig. 15).

A similar picture is observed for all other isochores. The degree of closeness of the argon spinodal found in this way in Ref. [92] to its positions found in Refs [90, 91] is illustrated in Fig. 8.

We note that the change in the slope of temperature dependences $D_{\mathrm{s}}^{(\phi)}(T)$ at spinodal points is explained naturally by 1) the formation of bubbles of the vapor phase and 2) the densification of the liquid phase, which is accompanied by a decrease in the self-diffusion coefficient of water molecules (see [92] for details). The higher the degree of instability, the faster bubbles form in the system, i.e., in system states under the spinodal, they form substantially

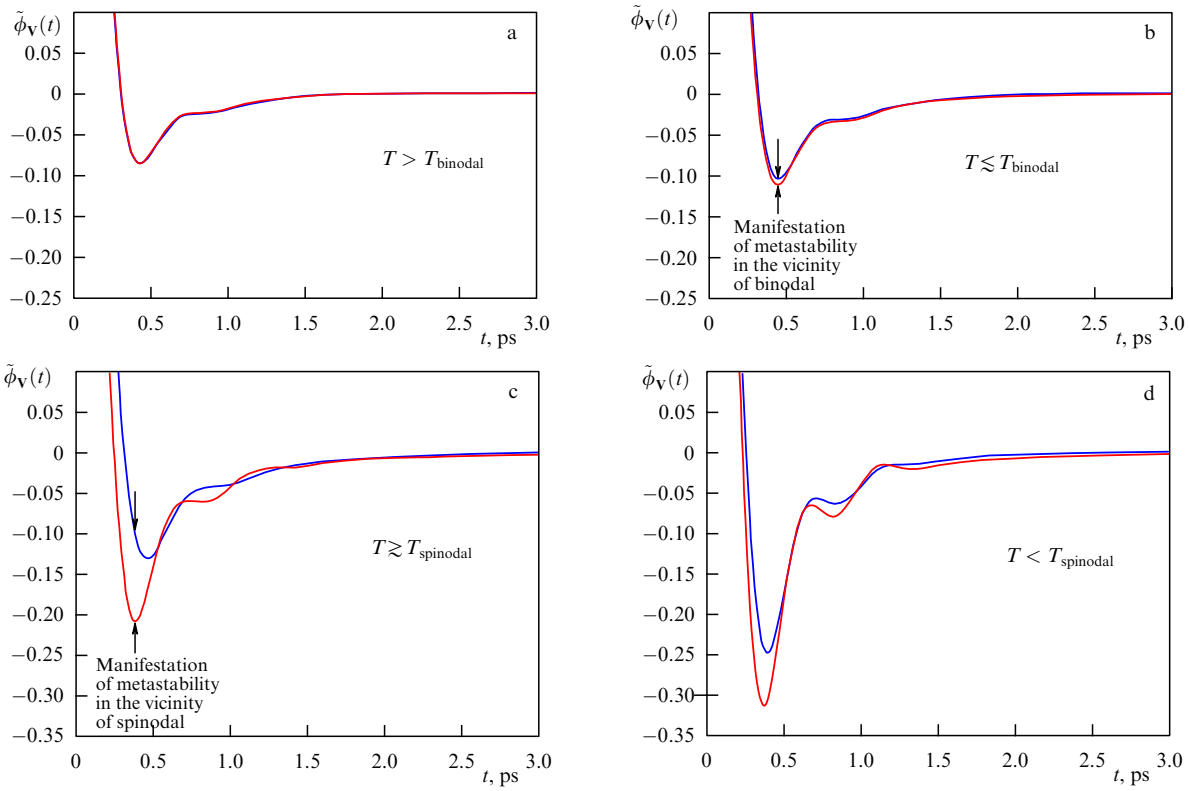

Figure 16. (Color online.) VACF of an argon molecule obtained with the help of equilibrium MD modeling (blue curve) and the VACF of an argon molecule additionally subjected to an instantaneous perturbation (red curve) on the isochore $\rho = 1.37$ g cm^{-3} for $T = 100$ K (a), $T = 80$ K (b), $T = 60$ K (c), and $T = 30$ K (d).

faster than in its metastable states. This is why a numerical experiment to find the binodal must be considerably longer, and the size of the particle ensemble in the cell must be sufficiently large.

To make the detection of the binodal position more efficient, it is desirable to introduce weak external perturbations into the modeling process of the VACF of argon molecules, or, in other words, to destroy the symmetry spontaneously. Such external actions include: 1) short-term contact with a perturbed twin system; 2) short-term stretching of a group of molecules close to one of the cell faces; 3) a small change in the coordinates or momenta of some group of molecules. None of these actions distort the behavior of the VACFM for stable argon states (Fig. 16a). If the state moves along the isochore into the region of metastable and absolutely unstable states, the distinctions between the equilibrium and 'perturbed' VACFs (the blue and red lines, respectively, in Fig. 16) become visible only for temperatures $T \leqslant T_{\text{binodal}}$ (Fig. 16b). Deeper in the region of metastable states, the distinctions between the equilibrium and 'perturbed' VACFs become more significant and reach a maximum in the vicinity of the spinodal (Fig. 16c). The lowering of temperature in the region under the spinodal is accompanied by a reduction in the difference between temporal dependences of equilibrium and 'perturbed' VACFs (Fig. 16d). Making use of the Green–Kubo relationships connecting the VACF with the self-diffusion coefficient, the temperature dependence of $D_{\text{s}}^{(\phi)}(T)$ is obtained for a perturbed ensemble on the isochore $\rho = 1.37$ g cm^{-3} (Fig. 15b). The points where the slope of $D_{\text{s}}^{(\phi)}(T)$ changes coincide with the upper and lower boundaries of metastable states (T_1, T_2) (Fig. 15b).

Table 9. Temperatures of binodal and spinodal of water.

ρ, g cm^{-3}	T_{b}, K [106]	T_{b}^{MD}, K	T_{s}, K [106]	T_{s}^{MD}, K
0.65	620	605	525	550
0.75	565	560	447	470
0.79	558	530	443	423

The value of T_1 proves to be close to the binodal temperature T_{b} for a given density, and T_2 proves to be close to the spinodal temperature T_{s}. The more prominent the change in the slope of the temperature dependence of $D_{\text{s}}^{(\phi)}(T)$ in the vicinity of the binodal, the further the isochore being studied is located from the critical isochore.

The temperature dependence of the self-diffusion coefficient in water behaves similarly. The temperatures of water spinodals and binodals found in this way on a set of isochores are presented in Table 9.

8. Similarity relations

In this section, we present the results obtained using similarity relations for the coefficients of self-diffusion and kinematic shear viscosity, and also for the MRT. The use of similarity relations for low-molecular liquids with spherical molecules, as in argon, is well accepted [107, 108]. This is why our main attention will be focused on liquids with dumbbell-shaped molecules such as in nitrogen, disk-shaped molecules as in benzene, and with hydrogen bonds similar to those formed between water molecules. We need to stress that this set of problems is tightly connected to the formation of universal tails in the VACF of molecules.

A key factor enabling the use of similarity relations for liquids with nonspherical molecules is their thermal rotation, which leads to self-averaging of intermolecular potentials and the formation of mean interaction potentials that are argon-like [83]. In this respect, we add that the description of the state of low-molecular liquids with the help of the Van der Waals equation is only possible because they are defined with a quite satisfactory accuracy by angular-mean interaction potentials that are close to the Lennard-Jones potential in their structure. As applied to liquid nitrogen and benzene, this question is discussed in Refs [83, 109], and for water and alcohols in Ref. [110].

In agreement with this, all kinematic coefficients mentioned above should satisfy the following similarity relations:

$$D_i(T_i) = \frac{\sigma_i}{\sigma_{\mathrm{Ar}}}\left(\frac{\varepsilon_i}{\varepsilon_{\mathrm{Ar}}}\frac{m_{\mathrm{Ar}}}{m_i}\right)^{1/2} D_{\mathrm{Ar}}(T_{\mathrm{Ar}})\,,$$
$$\nu_i(T_i) = \frac{\sigma_i}{\sigma_{\mathrm{Ar}}}\left(\frac{\varepsilon_i}{\varepsilon_{\mathrm{Ar}}}\frac{m_{\mathrm{Ar}}}{m_i}\right)^{1/2} \nu_{\mathrm{Ar}}(T_{\mathrm{Ar}})\,, \qquad (55)$$
$$T_i = \frac{\varepsilon_i}{\varepsilon_{\mathrm{Ar}}}T_{\mathrm{Ar}}\,, \quad i = \mathrm{Kr}\,, \mathrm{N_2}\,, \mathrm{C_6H_6}\,, \mathrm{H_2O}\,, \ldots\,.$$

Here, $\varepsilon_{\mathrm{Ar}}$ and σ_{Ar} are the parameters of the Lennard-Jones potential for argon and ε_i and σ_i are the parameters of effective Lennard-Jones potentials for nonspherical molecules. The effective interaction potentials $U_{\mathrm{a}}(r)$ arise after averaging of microscopic potentials $U(r, \Gamma_1, \Gamma_2)$ over the angular variables $\Gamma_i, i = 1, 2$,

$$\frac{1}{\Gamma^2}\int_\Gamma\int_\Gamma \exp\left(-\frac{U(r,\Gamma_1,\Gamma_2)}{k_{\mathrm{B}}T}\right)\mathrm{d}\Gamma_1\mathrm{d}\Gamma_2 = \exp\left(-\frac{U_{\mathrm{a}}(r)}{k_{\mathrm{B}}T}\right), \qquad (56)$$

with Γ the volume of phase space that corresponds to variables Γ_i. Such a definition of effective potential ensures the conservation of the second virial coefficient. The angle-averaged interaction potential $U_{\mathrm{a}}(r)$ can be rather satisfactorily approximated by a function with the structure of the Lennard-Jones potential.

In particular, for N_2 and O_2 the parameters of effective potentials take the following values [83]:

$$m_{\mathrm{N_2}} = 24\,, \quad \varepsilon_{\mathrm{N_2}} = 95.05\,, \quad \sigma_{\mathrm{N_2}} = 3.698\,,$$
$$m_{\mathrm{O_2}} = 32\,, \quad \varepsilon_{\mathrm{O_2}} = 117.5\,, \quad \sigma_{\mathrm{O_2}} = 3.58\,.$$

For water, the values of ε_{w} and σ_{w} that correspond to various SPC-type model interaction potentials are compiled in Table 10.

Figure 17 plots the dependences of the dimensionless coefficient of kinematic shear viscosity $\tilde{\nu}_i = [m_i/(\sigma_i^2\varepsilon_i)]^{1/2}\nu_i$ on the dimensionless temperature $\tilde{T}_i = T/\varepsilon_i$ for atomic liquids, in which case the similarity relations hold with high accuracy, as repeatedly mentioned in [13, 107]. The degree of agreement with similarity relations for liquids with dumbbell-shaped molecules (see Fig. 17) is somewhat reduced. For the vicinities of their triple points, it is naturally related to the weak influence of angular correlations.

Somewhat unexpected is the observation that the values of kinematic shear viscosity and the self-diffusion coefficient for water molecules also vary on their existence curves similarly to those for argon [84]. In fact, this implies that the temperature dependences of ν and D_{s} for water, as well as for argon, have nothing in common with the activation mechanism of thermal motion [111, 112]. Furthermore, a careful modeling of thermal motion of ions in crystalline iron in the work by Belonozhko [113] indicated that activation jumps are also absent in solids. Transitions of ions from node to node happen not as a jump, but through joint displacements of no fewer than 5–6 ions, i.e., collective mixing of the same type as described in Refs [41, 109] is taking place.

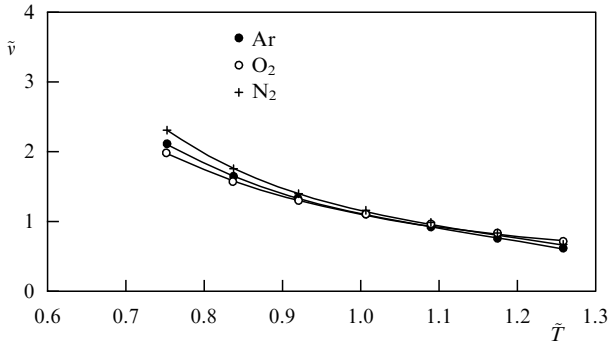

Figure 17. Dependence of $\tilde{\nu}_i$ on dimensionless temperature for Ar, N_2, and O_2 on their existence curves. The curves correspond to experimental data from Ref. [75], the symbols are the values computed by (55).

Table 10. Parameters of the Lennard-Jones potential that correspond to various model potentials for water molecules * [83].

	SPC	SPC/E	TIPS	TIP3P	SPCM	TIPSM	BM	BCM
ε_{w}	1.43	1.42	1.42	1.42	1.42	1.42	1.43	1.42
σ_{w}	2.78	2.78	2.77	2.77	2.77	2.75	2.94	2.93

* The quantity ε_{w} is presented in dimensionless form $\varepsilon_{\mathrm{w}} = \varepsilon_{\mathrm{a}}^{\mathrm{w}}/(k_{\mathrm{B}}T_{\mathrm{tr}}^{\mathrm{w}})$.

9. Conclusions

Summarizing the research on collective transport in liquids performed after the publication of the seminal work by I Z Fisher, we note that during this time:

(1) a consistent theory of thermal hydrodynamic fluctuations for Lagrangian variables of hydrodynamics was created [27–30, 40–49];

(2) based on this theory, explicit expressions were obtained for collective contributions in coefficients of self-diffusion and rotational diffusion of molecules of liquids;

(3) methods to determine the Maxwell relaxation time for viscous stresses in liquids were developed, and general limitations imposed on the MRT were formulated;

(4) a model-less method to estimate the relative value of the collective component in the self-diffusion coefficient was proposed;

(5) a general method to scan the collective drift of molecules in liquids was proposed that relies on studying the temperature dependence of the effective hydrodynamic radius of molecules;

(6) these results were generalized to the case of two-dimensional systems.

Additionally, based on an analysis of the long-term asymptotic decay of the VACFM:

(1) one more method was developed to determine shear viscosity in liquids and solutions, which complements the fundamental Green–Kubo methods [62, 63];

(2) it was found that the VACF of molecules of liquids demonstrates two types of universal behavior: a power-law long-term asymptotic form and exponential decay of its spectrum at sufficiently high frequencies;

(3) similarity relations for temperature dependences of basic kinetic coefficients were generalized for practically all low-molecular liquids, including water. It relies on using parameters of averaged intermolecular interaction potentials.

With the help of molecular dynamics methods:

(1) the Maxwell relaxation time for viscous stresses was determined. It was shown that only in the temperature range $T_{\rm tr} < T < T_*$, noticeably narrower ($T_* < T_{\rm c}$) than the existence range of the system liquid state, the MRT satisfies all necessary limitations;

(2) it was found that the relative value of collective contributions in the self-diffusion coefficient in various liquids increases with temperature and reaches 25%;

(3) it was shown that the characteristic functions constructed on the basis of molecule mean square displacement reach a plateau, which is a weighty argument for the existence of collective transport in fluids;

(4) it was demonstrated that it is possible to determine the leading power-law index of the repulsing component of the intermolecular interaction potential based on an analysis of high-frequency spectra of the VACFM.

The existence of vortex motions in a molecular system is explicitly demonstrated in Refs [114–119]. Reference [118] shows that the velocity field $\mathbf{u}(\mathbf{r}, t)$, which is obtained by averaging velocities of molecules over the volume of a liquid particle,

$$\mathbf{u}(\mathbf{r}, t) = \frac{1}{N(\mathbf{r})} \sum_{i=1}^{N(\mathbf{r})} \mathbf{V}_i(t)\,,$$

has a manifest vortical structure (here, $\mathbf{V}_i(t)$ is the velocity of the i-th molecule and $N(\mathbf{r})$ is the number of molecules in the volume of a liquid particle embracing the point $\mathbf{r}$). Unfortunately, a similarly transparent indication has thus far been missing for the potential component in the velocity field $\mathbf{u}(\mathbf{r}, t)$.

A series of studies [120–122] belonging to the same authors explores the character of mutual divergence of two particles that were initially at the distance $r_{12}(0)$ from each other. It is shown that the mean square distance between these particles $\Gamma_{12}(t) = \langle(\mathbf{r}_2(t) - \mathbf{r}_1(t))^2\rangle$ stays practically without change for about 60 ps if their initial distance $r_{12}(0)$ does not exceed 5–6 mean distances a between the particles. If $r_{12}(0) \gg (5-6)a$, then $\Gamma_{12}(t)$ increases practically from the very beginning, following the self-diffusion law,

$$\Gamma_{12}(t) \approx r_{12}^2(0) + 12 D_{\rm s} t\,,$$

which corresponds to an independent distancing of molecules from each other. Based on these results, the authors of Refs [120–122] conclude that 1) the appropriate radius of a Lagrangian particle r_* should be approximately $r_* \approx (1/2) r_{12}(0) \sim (2.5-3)a$; 2) and its lifetime $t_{\rm L} \approx 60$ ps. We note that the lifetime of a liquid particle estimated as the time of its disintegration due to self-diffusion processes,

$$t_{\rm L} \sim \frac{r_*^2}{12 D_{\rm s}} \sim 10^2 \text{ ps}\,,$$

has the same order of magnitude for $r_*(0) \sim (5-6)a$. These estimates are in quite satisfactory qualitative agreement with those obtained by us in the framework of the Lagrangian theory of thermal hydrodynamic fluctuations.

It is desirable to complement the universal character of the long-term asymptotic form of the VACF of molecules by mentioning the universality of the behavior of their spectral asymptotic form, which decays exponentially. In their formation, an important role is played by the notion of the hard component of collision between molecules defined by the repulsion forces. This component differs substantially from the more common component of the soft collision, which has a multiparticle nature in liquids and is governed mainly by intermolecular attraction forces. Since the repulsion forces are short-range, one may speculate about the sequence of hard binary collisions even in liquids, which lies at the core of their relatively simple description. This circumstance was first used in Ref. [102] and then substantially extended in Ref. [94] (see also [95]). Exponential high-frequency asymptotic forms are also intrinsic to the spectra of correlation functions which describe molecular light scattering in simple liquids [103–105, 123]. From an analysis of these asymptotic forms, it follows that, in addition to the commonly known contribution to the repulsion potential in atomic liquids,

$$U_{\rm R}(r) = \varepsilon \left(\frac{\sigma}{r}\right)^{12},$$

the expansion of $U_{\rm R}(r)$ in powers of $(\sigma/r)^m$ also includes terms among which the contribution with $m = 28$ dominates at small distances between particles [103–105]. This result is also confirmed by analyses of the equation of state of liquids at high pressure, exemplified by the Tate equation [124]. Only in the vicinity of triple points of liquids does $m \approx 12$ (see Refs [125–127]).

We stress that the values of reduced energy E (see Refs [94, 95]) satisfying the inequality $E \gg k_{\rm B}T$ correspond to sufficiently large frequency shifts in light molecular scattering (LMS) spectra. The most substantial changes in velocity and acceleration of a particle with reduced mass take place in a small narrow vicinity of the stop point, where the main role is played by the leading contribution to the repulsion potential. The high-frequency asymptotic forms of LMS spectra for this reason are some of the most efficient means to scan leading contributions in repulsing components of interaction potentials.

Appendix 1. Details of computer modeling of the velocity autocorrelation function for argon and water molecules

We briefly describe specific details related to modeling the temporal behavior of the VACF for argon and water molecules by molecular dynamics methods.

In the majority of situations, where the reconstruction of the VACF temporal profile for argon molecules was needed, we used an ensemble comprising 10^6 molecules (further referred to as a small ensemble) which interact among themselves through the Lennard-Jones potential

$$U(r) = 4\varepsilon \left[\left(\frac{\sigma}{r}\right)^{12} - \left(\frac{\sigma}{r}\right)^{6}\right]$$

with the parameters $\sigma = 0.3409$ nm and $\varepsilon/k_{\rm B} = 120.04$ K [128].

An especially large ensemble of molecules, including 27×10^6 particles, was only employed to study the long-time tails of the VACF of argon molecules in the low-frequency part of its spectrum.

Modeling was carried out with the help of the software package GROMACS 5.1 (GROningen Machine for Chemical Simulations 5.1) [129–131]. To integrate motion equations numerically, the fast Verlet algorithm was used [131]. In all computations, the integration time step did not exceed 4×10^{-16} s.

Particles fill a cell that provides a given system density. The dynamics inside the cell are subject to periodic boundary conditions. The linear cell size l_e is substantially larger than twice the radius r_I of intermolecular interactions, $l_e \gg 2r_I$. The size of the ensemble to be modeled was selected so that the period $\tau_c = l_e/c_l$ (c_l is the longitudinal sound speed in the system) of the largest scale acoustic oscillations always exceeded the characteristic time τ_s of correlations studied through simulations ($\tau_s < \tau_c$). The maximum radius of intermolecular interactions was taken to be equal to $r_I = 9\sigma$. The equilibrium values of pressure and density at a given density and temperature were in correspondence with the experimental equation of state of the system; the values of self-diffusion coefficients found from the analysis of the MSD of a molecule and by integration of the VACF are equal to each other.

Attention should be drawn to the fact that some of the conclusions formulated above are based on the analysis of long-term tails of the VACFM and low-frequency VACF spectra, which implies modeling the system behavior at times of the order of 20 ps. In this respect, it is particularly important to bring the properties of the model system into agreement with those that follow from the equation of state.

At its initial stage, the model system is an *NVE*-ensemble that relaxes to an equilibrium state. A quasistationary value of temperature is established in the system, which differs notably from the one given initially. The value of pressure is also substantially different from the experimental one. To bring the pressure to correct values, the *NVE*-ensemble obtained during the previous modeling stage is employed as an initial configuration of an *NPT*-ensemble using a chain of Nosé–Hoover thermostats [132, 133] and a Martyna–Tuckerman–Tobias–Klein barostat [134, 135]. To exclude substantial pressure fluctuations in the system, a large adaptation time is taken [131]. As a result, the model pressure and temperature slowly return to the required experimental values. Owing to the process substantial duration, the spatial distribution and the distribution of molecules over velocities stay mutually consistent, whereby large fluctuations are excluded in the system potential energy. On achieving the required values of pressure and temperature, the system density deviates but little from the experimental value. For instance, for $T = 100$ K, the experimental density is $\rho = 1.314$ g cm^{-3}, whereas the respective model value is $\rho = 1.321$ g cm^{-3}. As a result, the density of molecules at a given pressure and temperature deviates from the experimental one by less than 1%.

The final modeling stage is used to reconstruct the temporal profile of the VACFM. The *NPT*-ensemble equilibrated as described above is taken as an initial configuration to model the equilibrium molecular dynamics of an *NVE*-ensemble. The simulated model trajectories (evolving velocities and coordinates of ensemble particles) were stored every tenth step. To reconstruct the VACF, a set of at least 23,000 frames was used. The temporal window to compute the VACF (and the number of frames, respectively) were selected so as not to exceed the period of the largest-scale acoustic oscillations in the ensemble being studied. Why this is important is explained, for example, in Ref. [136]. Each dependence $\phi(t)$ used in the work is a result of averaging over six independent sets of MD trajectories.

Table 11. Values of parameters of the potential TIP4P/F [137].

Parameter	Value
ε	$93.2k_B$
σ, Å	3.1644
q_H/e	0.5564
D_r, kJ mol^{-1}	432.58
r_0, Å	0.9419
β, nm^{-1}	22.81
θ_0, degree	107.4
K_θ, kJ mol^{-1} rad^{-2}	367.81

To construct the VACF profile for water, an ensemble comprising 10^6 molecules was taken. The interaction between molecules was described in the framework of the four-point model TIP4P and the four-point elastic model TIP4P/F [137], which allows excitation of internal molecular oscillations (the distances r_{OH} between the oxygen and hydrogen ions and the angle formed by the bonds between O and H). As in the case of argon, the GROMACS 5.1 software package was used with an integrated amber99sb-ilbn force field, which naturally supports both models mentioned above [131]. The values of parameters for the potential TIP4P/F are given in Table 11.

The dynamic memory time τ_d [136, 138] is 21 ps. This implies that all the conclusions drawn from the analysis of the VACF temporal profile modeled at times $t < \tau_d$ can be considered physically grounded.

The relative error ε of MD simulations is given by the relationship

$$\varepsilon = 2\text{average}\left(\frac{|\phi_i(t) - \phi_j(t)|}{|\phi_i(t) + \phi_j(t)|}\right),$$

where averaging is carried out over all pairs i and j of various initial configurations. At large times, the VACF decays according to the known power law, which causes an increase in its relative error. For instance, in the time interval 3–6 ps, the mean relative error is $\varepsilon = 0.081$, but it reaches the value $\varepsilon = 0.237$ in the interval 10–15 ps. To smooth noise coming from the limited size of the ensemble studied, a Savitzki–Golay spline-filter [139] is used.

Appendix 2. Manifestations of dimer oscillations in the velocity autocorrelation function of the water molecule

The water dimer has six degrees of freedom, of which five correspond to the change in the orientation of water molecules, and the sixth one corresponds to the change in the distance between the centers of mass of the molecules. The appearance of the fine structure in the spectral density of the VACFM is related precisely to this degree of freedom.

Dimensionless frequencies of normal oscillations of an isolated dimer $\tilde{\omega}_k = \omega_k/\omega_0$, $\omega_0 = 10^{13}$ s^{-1}, $k = 1, 2, \ldots, 6$, are given in Table 12 [44].

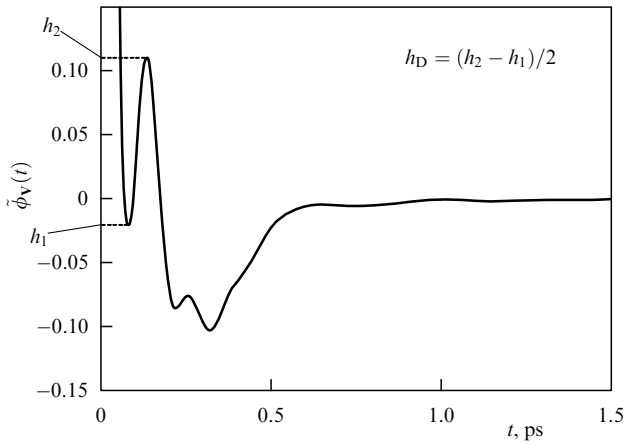

Figure 18. Finding the amplitude of dimer longitudinal oscillations.

Table 12. Dimensionless frequencies of normal oscillations of an isolated dimer.

	N_1	N_2	N_3	N_4	N_5	N_6
$\tilde{\omega}_k$	3.52	2.28	6.97	2.97	10.64	2.71

The normal coordinate that corresponds to oscillations in the distance between molecules in the dimer is denoted by the symbol N_1. We compare its oscillation frequency with the position $\tilde{\omega}_p$ of the small peak in Fig. 12. It can be seen that its frequency $\tilde{\omega}_p \approx 4.2$ practically coincides with the frequency of longitudinal oscillations of the isolated dimer.

From the temperature dependence of the dimer oscillation amplitude $h_D(T)$ (Fig. 18), it follows that dimer longitudinal oscillations can be reliably recorded for temperatures $T < T_D$, where $T_D \approx 450$ K.

References

1. Fisher I Z *Sov. Phys. JETP* **34** 878 (1972); *Zh. Eksp. Teor. Fiz.* **61** 1647 (1971)
2. Fisher I Z, Zatovskii A V, Malomuzh N P *Sov. Phys. JETP* **38** 146 (1974); *Zh. Eksp. Teor. Fiz.* **65** 297 (1973)
3. Malomuzh N P, Fisher I Z *Zh. Strukt. Khim.* **14** 1105 (1973)
4. Malomuzh N P, Fisher I Z, in *Fizika Zhidkogo Sostoyaniya* (Physics of Liquid State) Issue 1 (Ed.-in-Chief A Z Golik) (Kiev: Izd. pri Kievskom Univ., 1973) p. 33
5. Alder B J, Wainwright T E *Phys. Rev. Lett.* **18** 988 (1967)
6. Alder B J, Wainwright T E *Phys. Rev. A* **1** 18 (1970)
7. Alder B J, Gass D M, Wainwright T E *J. Chem. Phys.* **53** 3813 (1970)
8. Wainwright T E, Alder B J, Gass D M *Phys. Rev. A* **4** 233 (1971)
9. van der Hoef M A, Frenkel D *Phys. Rev. Lett.* **66** 1591 (1991)
10. van der Hoef M A, Frenkel D, Lodd A J C *Phys. Rev. Lett.* **67** 3459 (1991)
11. Lowe C P, Frenkel D *Physica A* **220** 251 (1995)
12. Lowe C P, Frenkel D, Masters A J *J. Chem. Phys.* **103** 1582 (1995)
13. Résibois P, De Leener M *Classical Kinetic Theory of Fluids* (New York: Wiley, 1977)
14. Ernst M H, Hauge E H, van Leewen J M J *Phys. Rev. Lett.* **25** 1254 (1970)
15. Ernst M H, Hauge E H, van Leewen J M J *Phys. Lett. A* **34** 419 (1971)
16. Ernst M H, Hauge E H, van Leewen J M J *Phys. Rev. A* **4** 2055 (1971)
17. Kawasaki K *Phys. Lett. A* **32** 379 (1970)
18. Gaskell T, March N H *Phys. Lett. A* **33** 460 (1970)
19. Ernst M H, Dorfman J R *Physica* **61** 157 (1972)
20. Dorfman J R, Cohen E G D *Phys. Rev. A* **12** 292 (1975)
21. Mazenko C F *Phys. Rev. A* **7** 209 (1973)
22. Bogolyubov N N *Fiz. Elem. Chast. At. Yad.* **9** 501 (1978)
23. Kadanoff L P, Martin P *C Ann. Physics* **24** 419 (1963)
24. Puff R D, Gillis N S *Ann. Physics* **46** 364 (1968)
25. McIntyre D, Sengers J V, in *Physics of Simple Liquids* (Eds H N V Temperley, J S Rowlinson, G S Rushbrooke) (Amsterdam: North-Holland, 1968) p. 447
26. Forster D *Hydrodynamic Fluctuations, Broken Symmetry, and Correlation Functions* (Redwood City, CA: Addison-Wesley, Advanced Book Program, 1990)
27. Lokotosh T V, Malomuzh N P *Physica A* **286** 474 (2000)
28. Lokotosh T V, Malomuzh N P *J. Mol. Liq.* **93** 95 (2001)
29. Lokotosh T V, Malomuzh N P, Shakun K S *J. Mol. Liq.* **96–97** 245 (2002)
30. Lokotosh T V, Malomuzh N P, Shakun K S *J. Chem. Phys.* **118** 10382 (2003)
31. Zwanzig R, Bixon M *Phys. Rev. A* **2** 2005 (1970)
32. Zwanzig R, Bixon M *J. Fluid Mech.* **69** 21 (1975)
33. Dorfman J R, Cohen E G D *Phys. Rev. A* **6** 776 (1972)
34. Pomeau Y *Phys. Rev. A* **5** 2569 (1972)
35. Pomeau Y, Résibois P *Phys. Rep.* **19** 63 (1975)
36. Hansen J P, McDonald I R *Theory of Simple Liquids* (New York: Academic Press, 1991)
37. McDonough A, Russo S P, Snook I K *Phys. Rev. E* **63** 026109 (2001)
38. Dib R F A, Ould-Kaddour F, Levesque D *Phys. Rev. E* **74** 011202 (2006)
39. Oskotskii V S *Sov. Phys. Solid State* **5** 789 (1963); *Fiz. Tverd. Tela* **5** 1082 (1963)
40. Bulavin L A, Lokotosh T V, Malomuzh N P *J. Mol. Liq.* **137** 1 (2008)
41. Lokotosh T V et al. *Ukr. Fiz. Zh.* **60** 8697 (2015)
42. Malomuzh N P, Fisher I Z *Ukr. Fiz. Zh.* **19** 5851 (1974)
43. Bulavin L a et al. *Ukr. Fiz. Zh.* **49** 6556 (2004)
44. Bulavin L A, Malomuzh N P, Pankratov K N *Zh. Strukt. Khim.* **47** 3554 (2006)
45. Bulavin L A, Malomuzh N P, Pankratov K N *Zh. Strukt. Khim.* **47** 52 (2006)
46. Lokotosh T V, Malomuzh N P, Pankratov K N *J. Chem. Eng. Data* **55** 2021 (2010)
47. Lokotosh T V, Malomuzh N P, Pankratov K N *Zh. Fiz Khim.* **57** 1120 (2011)
48. Lokotosh T V, Malomuzh N P, Pankratov K N *Zh. Strukt. Khim.* **54** S197 (2013)
49. Malomuzh N P, Makhlaichuk V N *Russ. Metall.* (8) 750 (2019); *Rasplavy* (5) 562 (2018)
50. Dexter A R, Matheson A J *J. Chem. Phys.* **54** 203 (1971)
51. Verlet L *Phys. Rev.* **159** 98 (1967)
52. Mason W P *Physical Acoustics* (New York: Academic Press, 1964)
53. Bulavin L A et al. *Ukr. Fiz. Zh.* **31** 1703 (1986)
54. Bulavin L A et al. *Zh. Fiz. Khim.* **61** 3270 (1897)
55. Bulavin L A et al. *Ukr. Fiz. Zh.* **50** 939 (2005)
56. Malomuzh N P, Shakun K S *J. Mol. Liq.* **293** 111413 (2019)
57. Vergeles M, Szamel G *J. Chem. Phys.* **110** 3009 (1999)
58. Ruckenstein E, Liu H *Ind. Eng. Chem. Res.* **36** 3927 (1997)
59. Wang L *EPJ Web Conf.* **151** 02004 (2017)
60. Chauhan A S, Ravi R, Chhabra R P *Chem. Phys.* **252** 227 (2000)
61. Zubarev D N *Nonequilibrium Statistical Thermodynamics* (New York: Consultants Bureau, 1974); Translated from Russian: *Neravnovesnaya Statisticheskaya Termodinamika* (Moscow: Nauka, 1971)
62. Green M S *J. Chem. Phys* **22** 398 (1954)
63. Kubo R *J. Phys. Soc. Jpn.* **12** 570 (1957)
64. Grechanyi O A *Stokhasticheskaya teoriya neobratimykh protsessov* (Stochastic Theory of Irreversible Processes) (Kiev: Naukova Dumka, 1989)
65. Slyusarenko Yu V *Ukrainskii Fiz. Zh.* **28** 774 (1983)
66. Sokolovsky A I *Ukrainskii Fiz. Zh.* **45** 545 (2000)
67. Sokolovsky A I *Condens. Matter Phys.* **9** 415 (2006)
68. Peletminsky S V, Slusarenko Yu V *Physica A* **210** 165 (1994)
69. Peletminskii S V, Slyusarenko Yu V, Sokolovsky A I *Physica A* **326** 412 (2003)
70. Rudyak V Ya et al. *High Temp.* **46** 30 (2008); *Teplofiz. Vys. Temp.* **46** 35 (2008)
71. Morse P M, Feshbach H *Methods of Theoretical Physics* (New York: McGraw-Hill, 1953)

72. Stepišnik J et al. *Eur. Phys. J. B* **91** 293 (2018)
73. Hartkamp R, Daivis P J, Todd B D *Phys. Rev. E* **87** 032155 (2013)
74. van der Gulik P S *Physica A* **256** 39 (1998)
75. National Institute of Standards and Technology. Standard Reference Database 69: NIST Chemistry WebBook (accessed 5 December 2018). Models and Tools. Thermophysical Properties of Fluid Systems, http://webbook.nist.gov/chemistry/fluid
76. Rumble J R (Ed.) *CRC Handbook of Chemistry and Physics* (Boca Raton, FL: CRC Press, 2018)
77. Vogt C, Laihem K, Wiebusch C *J. Acoust. Soc. Am.* **124** 3613 (2008)
78. Mills R *J. Phys. Chem.* **77** 685 (1973)
79. Harris K R, Woolf L A *J. Chem. Soc. Faraday Trans. 1* **76** 377 (1980)
80. Corbett J W, Wang J H *J. Chem. Phys.* **25** 422 (1956)
81. Naghizadeh J, Rice S A *J. Chem. Phys.* **36** 2710 (1962)
82. Laghaei R, Nasrabad A E, Eu *B C J. Phys. Chem. B* **109** 5873 (2005)
83. Makhlaichuk P V, Makhlaichuk V N, Malomuzh N P *J. Mol. Liq.* **225** 577 (2017)
84. Malomuzh N P, Makhlaichuk V N *J. Mol. Liq.* **295** 111729 (2019)
85. Rahman A *Phys. Rev.* **136** A405 (1964)
86. Rahman A, Stillinger F H *J. Chem. Phys.* **55** 3336 (1971)
87. Adebayo G A et al. *Pramana* **75** 523 (2010)
88. Balucani U, Brodholt J P, Vallauri R *J. Phys. Condens. Matter* **8** 6139 (1996)
89. Lie G C, Clementi E *Phys. Rev. A* **33** 2679 (1986)
90. Kuksin A Yu, Norman G E, Stegailov V V *High Temp.* **45** 37 (2007); *Teplofiz. Vys. Temp.* **45** 43 (2007)
91. Baidakov V G, Skripov V P *Sov. Phys. JETP* **48** 509 (1978); *Zh. Eksp. Teor. Fiz.* **75** 1007 (1978)
92. Malomuzh N P, Shakun K S *J. Mol. Liq.* **235** 155 (2017)
93. Wright N J, Makri N *J. Chem. Phys.* **119** 1634 (2003)
94. Troyanovskii V S *Sov. Phys. J.* **29** 552 (1986); *Izv. Vyssh. Ucheb. Zaved. Fiz.* (7) 59 (1986)
95. Bardik V Yu, Malomuzh N P, Shakun K S *J. Chem. Phys.* **136** 244511 (2012)
96. Grzybowski A et al. *J. Chem. Phys.* **133** 161101 (2010)
97. Roland C M, Feldman J L, Casalini R *J. Non-Cryst. Solids* **352** 4895 (2006)
98. Labinov M S, Sysoev V M, Chalyi A V *Teplofiz. Vys. Temp.* **20** 1194 (1982)
99. Labinov M S, Sysoev V M, Chalyi A V *Zh. Strukt. Khim.* **24** (1) 88 (1983)
100. Bardik V Yu, Sysoev V M *Low Temp. Phys.* **24** 602 (1998); *Fiz. Nizk. Temp.* **24** 797 (1998)
101. Rice S A, Allnatt A *R J. Chem. Phys.* **34** 2144 (1961)
102. Temperley H N V, Rowlinson J S, Rushbrooke G S (Eds) *Physics of Simple Liquids* (Amsterdam: North-Holland Publ. Co., 1968); Translated into Russian: *Fizika Prostykh Zhidkostei* (Moscow: Mir, 1971)
103. Bardic V Yu et al., in *Soft Matter under Exogenic Impacts* (NATO Science Series II, Mathematics, Physics and Chemistry, Vol. 242, Eds J Rzoska, V A Mazur) (Dordrecht: Springer, 2007)
104. Bardic V Yu, Malomuzh N P, Sysoev V M *J. Mol. Liq.* **120** 27 (2005)
105. Bardic V Yu et al. *J. Mol. Liq.* **127** 96 (2006)
106. Boulais E, Ph.D. Thesis (Montréal: Univ. de Montréal, Ecole Polytechnique de Montréal, 2013)
107. Croxton C A *Liquid State Physics — a Statistical Mechanical Introduction* (London: Cambridge Univ. Press, 1974); Translated into Russian: *Fizika Zhidkogo Sostoyaniya. Statisticheskoe Vvedenie* (Moscow: Mir, 1978)
108. Fisher I Z *Statistical Theory of Liquids* (Chicago, IL: Univ. of Chicago Press, 1964); Translated from Russian: *Statisticheskaya Teoriya Zhidkostei* (Moscow: Gos. Izd. Fiz.-Mat. Lit., 1961)
109. Makhlaichuk V M *Ukr. J. Phys.* **63** 986 (2018)
110. Gotsul'skii V Ya, Malomuzh N P, Chechko V E *Russ. J. Phys. Chem. A* **92** 1516 (2018); *Zh. Fiz. Khim.* **92** 1268 (2018)
111. Eyring H *J. Chem. Phys.* **4** 283 (1936)
112. Frenkel J *Kinetic Theory of Liquids* (Oxford: The Claredon Press, 1946); Translated from Russian: *Kineticheskaya Teoriya Zhidkostei* (Leningrad: Nauka, 1975)
113. Belonoshko A B et al. *Nat. Geosci.* **10** 312 (2017)
114. Dymond J H, Alder B J *Ber. Bunsengesell. phys. Chem.* **75** 394 (1971)
115. Verle L, in *Molecular Motion in Liquids* (Ed. J Lascombe) (Dordrecht: Springer, 1974)
116. Davies M, Evans M W, in *Dielectric and Related Molecular Processes* Vol. 3 (Ed. M Davies) (London: Burlington House, 1977) p. 1
117. Higo J et al. *Proc. Natl. Acad. Sci. USA* **98** 5961 (2001)
118. Malenkov G G, Naberukhin Yu I, Voloshin V P *Zh. Ross. Khim. Obshch. im. D I Mendeleeva* **53** 25 (2009)
119. Doostmohammadi A et al. *Nat. Commun.* **7** 10557 (2016)
120. Naberukhin Yu I, Voloshin V P *Zh. Strukt. Khim.* **48** 1066 (2007)
121. Malenkov G G, Naberukhin Yu I, Voloshin V P *Zh. Fiz. Khim.* **86** 1485 (2012)
122. Voloshin V P, Malenkov G G, Naberukhin Yu I *Zh. Strukt. Khim.* **54** (Suppl. 2) S233 (2013)
123. Bardik V Yu, Shakun K S *Ukr. Fiz. Zh.* **50** 404 (2005)
124. Golik A Z, Sysoev V M *Teplofiz. Vys. Temp.* **21** 454 (1983)
125. Stishov S M *Sov. Phys. Usp.* **18** 625 (1975); *Usp. Fiz. Nauk* **114** 3 (1974)
126. Pedersen U R, Schrøder T B, Dyre J C *Phys. Rev. Lett.* **105** 157801 (2010)
127. Friisberg I M, Costigliola L, Dyre J C *J. Chem. Sci.* **129** 919 (2017)
128. Oostenbrink C et al. *J. Comput. Chem.* **25** 1656 (2004)
129. Van der Spoel D et al. *J. Comput. Chem.* **26** 1701 (2005)
130. Swope W C et al. *J. Chem. Phys.* **76** 637 (1982)
131. Abraham M et al. *GROMACS. Groningen Machine for Chemical Simulations. Reference Manual Version 2018* (Groningen: Department of Biophysical Chemistry, Univ. of Groningen, 2018) p. 265
132. Nosé S *J. Chem. Phys.* **81** 511 (1984)
133. Hoover W G *Phys. Rev. A* **31** 1695 (1985)
134. Martyna G J, Tobias D J, Klein M L *J. Chem. Phys.* **101** 4177 (1994)
135. Martyna G J et al. *Mol. Phys.* **87** 1117 (1996)
136. Frenkel D, Smit B *Understanding Molecular Simulation: From Algorithms to Applications* 2nd ed. (San Diego: Academic Press, 2002)
137. González M A, Abascal J L F *J. Chem. Phys.* **135** 224516 (2011)
138. Kuksin A Y et al. *Mol. Simul.* **31** 1005 (2005)
139. Blanchet G, Charbit M *Digital Signal and Image Processing Using Matlab* (London: ISTE Ltd., 2006)